

Oral Microalgae-Nano Integrated System against Radiation-Induced Injury

Dongxiao Zhang, Jian He, Jiarong Cui, Ruoxi Wang, Zhe Tang,* Hongyu Yu,* and Min Zhou*



Cite This: *ACS Nano* 2023, 17, 10560–10576



Read Online

ACCESS |



Metrics & More



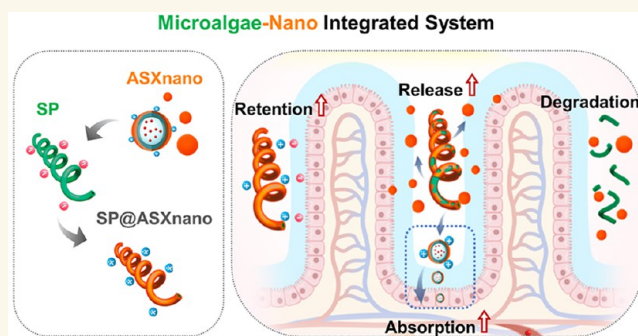
Article Recommendations



Supporting Information

ABSTRACT: The increasing applications of ionizing radiation in society raise the risk of radiation-induced intestinal and whole-body injury. Astaxanthin is a powerful antioxidant to reduce the reactive oxygen generated from radiation and the subsequent damage. However, the oral administration of astaxanthin remains challenging owing to its low solubility and poor bioavailability. Herein, we facilely construct an orally used microalgae-nano integrated system (SP@ASXnano) against radiation-induced intestinal and whole-body injury, combining natural microalgae *Spirulina platensis* (SP) with astaxanthin nanoparticles (ASXnano). SP and ASXnano show complementation in drug delivery to improve distribution in the intestine and blood. SP displays limited gastric drug loss, prolonged intestinal retention, constant ASXnano release, and progressive degradation. ASXnano improves drug solubility, gastric stability, cell uptake, and intestinal absorption. SP and ASXnano have synergy in many aspects such as anti-inflammation, microbiota protection, and fecal short-chain fatty acid up-regulation. In addition, the system is ensured with biosafety for long-term administration. The system organically combines the properties of microalgae and nanoparticles, which was expected to expand the medical application of SP as a versatile drug delivery platform.

KEYWORDS: micro-nano system, microalgae, astaxanthin, nanoparticle, radiation injury



INTRODUCTION

Radioactive materials and ionizing radiation (RT) appear widely in people's life since they have been applied in various aspects of modern society including nuclear energy, radiodiagnosis, radiotherapy, agriculture, and industry.^{1–3} Despite the beneficial applications, ionizing radiation can result in various health damages. In cases such as radiotherapy or nuclear accident, the radiosensitive organs would be exposed and cause a series of structural impairments and functional disorders.⁴ Among the severe side effects caused by clinical cancer radiotherapy, small intestinal injury is difficult to avoid and relieve since the small intestine is large in volume and highly sensitive to radiation.⁵ In accidental radiation exposure, the whole body could be injured, therefore leading to multiple lesions and even death.^{6,7} Therefore, effective formulations for intestinal and whole-body radioprotection are urgently required. Since the intestine is the main organ to absorb drugs into the blood, the intestinal distribution and absorption of the effective drug would be vital and significant to both intestinal and whole-body radioprotection.

Many antioxidative agents have been explored as radioprotectants because reactive oxygen species (ROS) generation is a critical mechanism of radiation-induced cellular injury.^{8,9}

Astaxanthin (ASX) is one of the strongest antioxidants with high oxygen radical absorbance capacity,¹⁰ which has been reported to have benefits in radiation-induced lesions.^{11–13} Furthermore, ASX has other functions including anti-inflammation, immune regulation, gut microbiota regulation, etc.^{14,15} However, the water insolubility, instability (in acid, oxygen, heat, and light), and low bioavailability of ASX hindered the construction of its oral formulation.¹⁶ Although the strategies to form micro- or nanoencapsulation could improve the oral bioavailability of ASX as reported previously,^{17–22} whether their application can achieve effective intestinal and systemic protection is unknown.

As a natural microalga 200–500 μm in size and helical shape, *Spirulina platensis* (*S. platensis*, SP) has been previously applied as a microcarrier for the construction of oral drug delivery systems, which could effectively improve the intestinal drug retention, slow release, and biodistribution.^{23,24} Importantly, the

Received: February 16, 2023

Accepted: May 1, 2023

Published: May 30, 2023



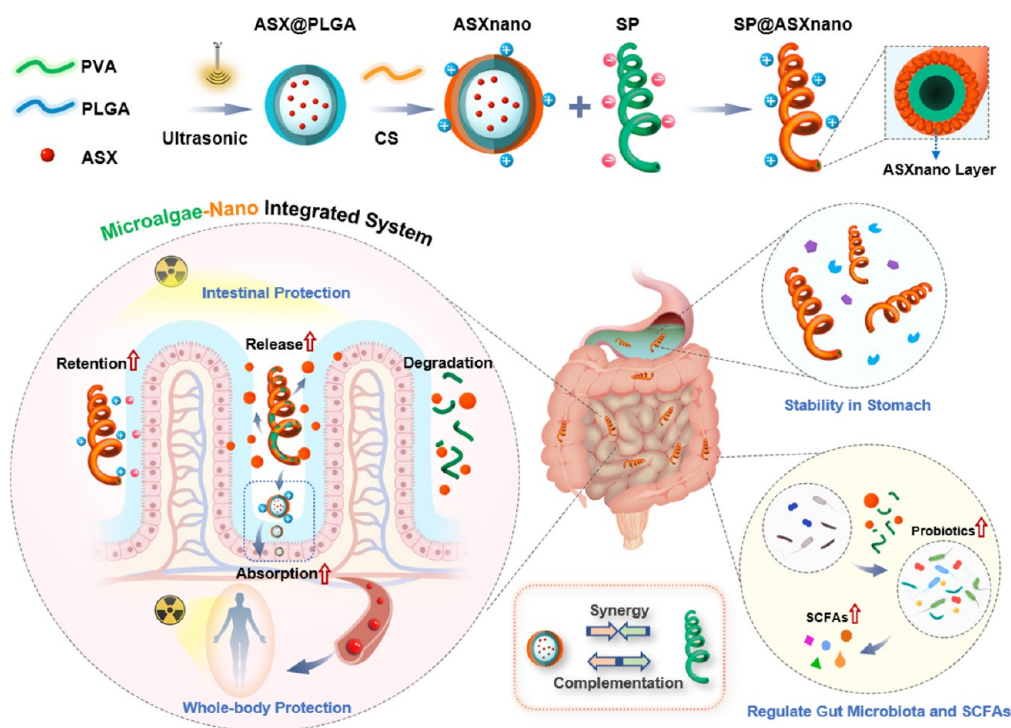


Figure 1. Schematic illustration showing the synthesis and action mechanisms of the microalgae-nano integrated system SP@ASXnano against radiation-induced intestinal and whole-body injury. The system combines the nanoparticles of astaxanthin (ASXnano) with microalgae SP through electrostatic adsorption. On one side, SP and ASXnano show complementation in drug delivery to improve the drug distribution in the intestine and blood: SP prolongs the retention and constantly releases ASXnano along the intestinal tract; ASXnano improves drug solubility, gastric stability, and intestinal absorption. On the other side, SP and ASXnano have synergy in anti-inflammation, microbiota protection, and fecal SCFAs up-regulation. PVA, poly(vinyl alcohol); PLGA, poly(lactic-co-glycolic acid); ASX, astaxanthin; CS, chitosan; ASXnano, the nanoparticle of ASX; SP, *Spirulina platensis*; ROS, reactive oxygen species; SCFA, short-chain fatty acid.

negatively charged surface of SP can attract molecules/particles with opposite charges, making it a highly adaptable microcarrier for the facile synthesis of many delivery systems.^{24–26} Moreover, SP has been proven to have various benefits, such as nutrient supplementation, anti-inflammation, gut microbiota, and metabolite regulation.^{27–31} Therefore, the strategy of combining SP with ASX may have great potential in radioprotection.

Herein, we designed an orally used microalgae-nano integrated system for intestinal and systemic radioprotection (Figure 1). The positively charged chitosan/PLGA nanoparticles of ASX (ASXnano) were attached to the natural negatively charged surface of the microalgae SP to construct the SP@ASXnano system. The strategy facilely reached a high loading efficiency without destroying the structures and bioactivities of SP. The *in vitro* and *in vivo* tests revealed the system's multiple advantages, in which microalgae SP and ASX nanoparticles showed complementation in drug delivery, meanwhile showing synergy in radioprotective effects. First, the complementation of SP and ASXnano significantly improved the drug distribution in the intestine and blood. SP could provide limited gastric drug loss, prolonged intestinal retention, constant ASXnano release, and progressive degradation. ASXnano could enhance drug solubility, gastric stability, cell uptake, and intestinal absorption. Second, SP and ASXnano have synergy in many aspects, such as anti-inflammation, microbiota protection, and fecal short-chain fatty acid (SCFA) up-regulation, reaching stronger radioprotective outcomes. As a result, the system exhibited more effective intestinal and systemic radioprotection than the single use of ASX as well as

its nanoparticle. It was also ensured with biosafety for long-term administration.

RESULTS AND DISCUSSIONS

Synthesis and Characterization of SP@ASXnano. We first loaded ASX into poly(lactic-co-glycolic acid) (PLGA) to form ASX@PLGA particles and then coated them with a chitosan (CS) layer to prepare ASXnano particles (Figure 2A), in which the zeta potential was reversed from -8.6 mV to $+67.3$ mV (Figure S1). The prepared ASXnano particles had a spherical shape (Figure 2B) and about a 203.2 nm hydrodynamic diameter (Figure 2C). The encapsulation efficiency (EE) of ASX in ASXnano was 95.5%. Compared with the insoluble ASX powder, ASXnano particles showed excellent dispersibility in an aqueous solution (Figure 2D). Furthermore, ASXnano particles could slowly release ASX into the simulated gastric and intestinal fluid (SGF and SIF) (Figure 2E). The drug release speed in acidic SGF was slower than that in neutral SIF, indicating less drug loss in the stomach.

Based on electrostatic adsorption between the positively charged ASXnano and the negative surface of SP, the preparation of the micro-nano system could be facilely achieved. The successful synthesis of SP@ASXnano could be observed from macro to micro dimensions (Figure 2F). The photographs of the suspension and the microscope images showed that the loading of ASXnano particles caused a color change of SP (from green to red) without destroying its structure. And the SEM images of SP@ASXnano displayed that a mass of ASXnano particles adhered to its surface and covered up the whole SP cell. The zeta potential test (Figure 2G) revealed that electrostatic

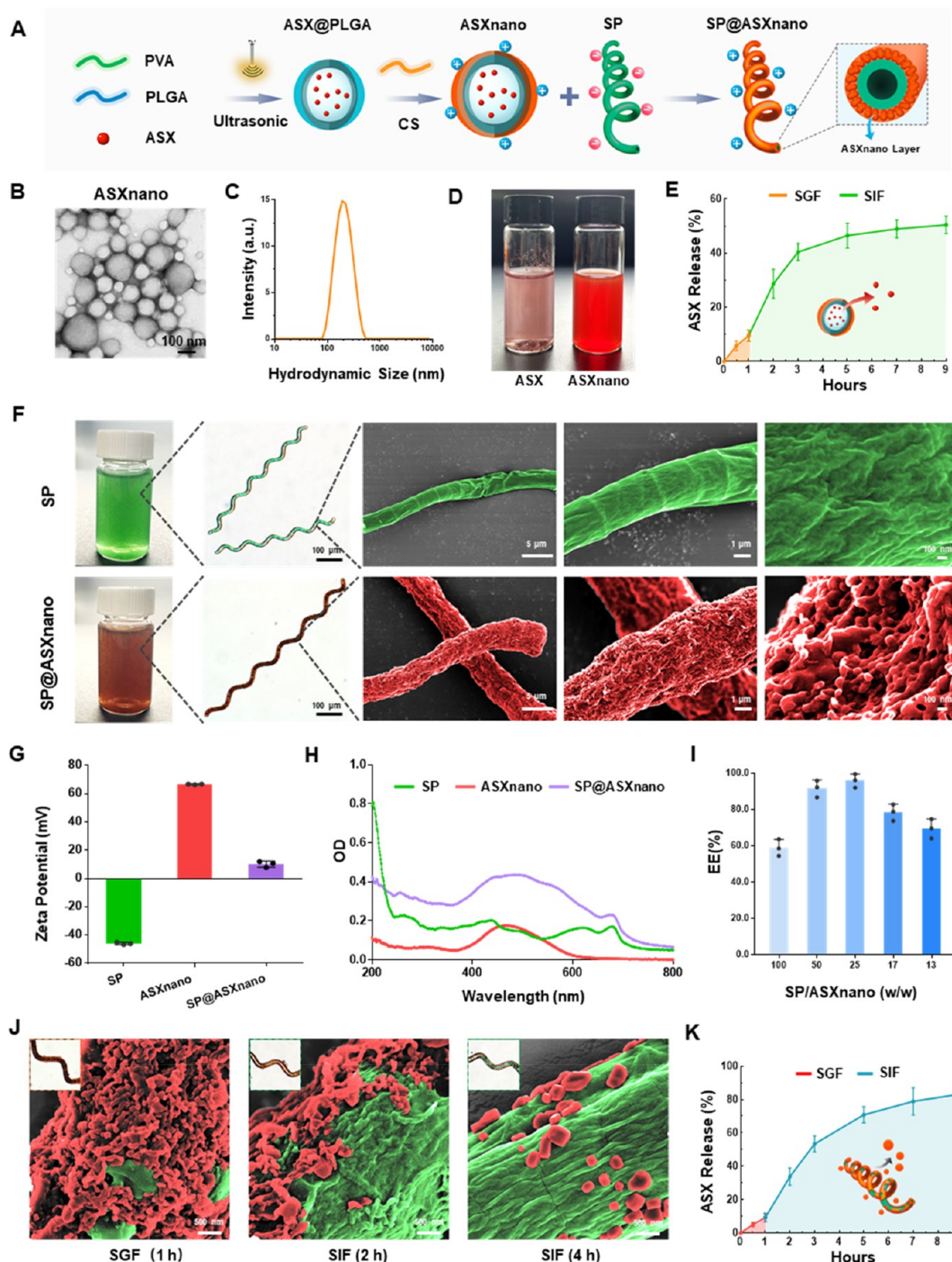


Figure 2. Synthesis and characterization of SP@ASXnano. (A) Synthesis of SP@ASXnano. PVA, poly(vinyl alcohol); PLGA, poly(lactic-co-glycolic acid); ASX, astaxanthin; CS, chitosan; SP, *Spirulina platensis*. (B) TEM image of ASXnano particles. (C) Hydrodynamic size distribution of ASXnano particles. (D) The water solution of ASX powder and ASXnano particles. (E) Releasing curves of ASX from ASXnano in SGF (simulated gastric fluid) and SIF (simulated intestinal fluid) ($n = 3$). Data are presented as means \pm SD. (F) Photographic, microscope, and SEM images (pseudocolor) of SP and SP@ASXnano. (G) Zeta potential of SP, ASXnano, and SP@ASXnano ($n = 3$). Data are presented as means \pm SD. (H) Ultraviolet spectra of SP, ASXnano, and SP@ASXnano. (I) Encapsulation efficiency (EE) under different weight ratios of SP:ASXnano ($n = 3$). Data are presented as means \pm SD. (J) Microscope and SEM images (pseudocolor) of SP@ASXnano after being treated by SGF or SIF for different durations. (K) Releasing curves of ASX from SP@ASXnano in SGF and SIF ($n = 3$). Data are presented as means \pm SD.

adsorption between the positively charged ASXnano particles (+66.7 mV) and the negatively charged SP (−46 mV) drove the synthesis of SP@ASXnano (+10.2 mV) as expected. The UV spectra (Figure 2H) also confirmed the successful assembly since SP@ASXnano presented the characteristic absorption peaks of SP as well as ASX. According to the encapsulation

efficiency data in Figure 2I and Figure S3, the optimal SP/ASXnano weight ratio (25:1) and loading time (15 min) were respectively determined.

To explore the drug-releasing profile of SP@ASXnano in the gastrointestinal environment, SP@ASXnano was treated by SGF for 1 h before being transferred into SIF for 4 h. As shown in

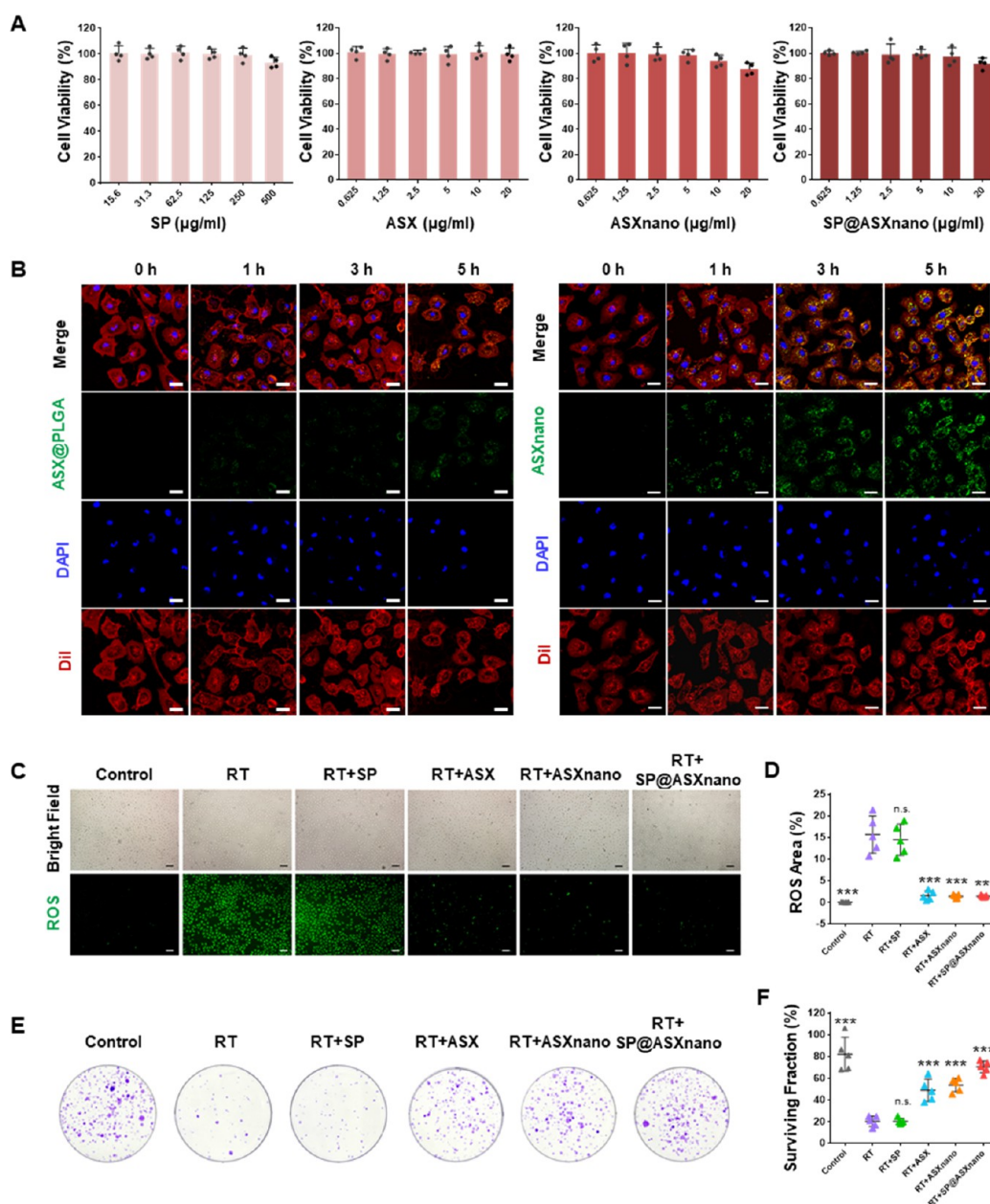


Figure 3. In vitro toxicity, antioxidation, and radioprotection. (A) Viabilities of IEC-6 cells after the incubation with different concentrations of SP, ASX, ASXnano, and SP@ASXnano for 24 h ($n = 4$). Data are presented as means \pm SD. (B) Fluorescence images of IEC-6 cells after the incubation with ASX@PLGA and ASXnano, respectively, for different durations (green, FITC-labeled ASXnano particles; blue, cell nuclei stained by DAPI; red, cell membrane stained by DiI). Scale bar, 20 μ m. (C) The bright field images and ROS fluorescence (green) images of IEC-6 cells that were exposed to 6 Gy X-ray (RT) after the incubation with different materials for 6 h. Scale bar, 100 μ m. (D) The fluorescence area measured in ROS fluorescence images ($n = 5$). Data are presented as means \pm SD; *, p vs RT group; *, $p < 0.05$, **, $p < 0.01$, ***, $p < 0.001$, n.s., no significance. (E) Surviving colonies of IEC-6 cells after different treatments. (F) The quantification of surviving colonies' fraction ($n = 5$). Data are presented as means \pm SD; *, p vs RT group; *, $p < 0.05$, **, $p < 0.01$, ***, $p < 0.001$, n.s., no significance.

Figure 2J, the microscope and SEM images of SP@ASXnano barely displayed the influence of SGF on the surface ASXnano particles, indicating its resistance to a harsh gastric environment. By contrast, the SP@ASXnano treated by SIF for 2 h showed a lighter red color and remained with fewer nanoparticles on its surface. After 2 more hours, only a few ASXnano particles remained, indicating a stepwise detachment of ASXnano particles from SP@ASXnano in the intestinal environment. Furthermore, the release curves of ASXnano from SP@ASXnano verified that the release speed of ASXnano in SGF was slower than that in SIF (Figure 2K). This might be

attributed to the electric potential changes of the ASXnano's chitosan coating, which tends to be more positive in acid and less positive in an alkaline fluid.^{32–34} As a result, the binding force (electrostatic interaction) between SP and ASXnano would be stronger in acid gastric fluid, allowing SP@ASXnano to avoid excessive drug loss in the stomach.

In Vitro Toxicity and Radioprotective Effect. Rat normal small intestinal epithelium cells (IEC-6) (Figure 3), mice monocyte-macrophages (RAW264.7) (Figures S6, S7), and human hepatic stellate cells (LX-2) (Figures S8, S9) were employed for in vitro tests. There was no obvious toxicity to cell

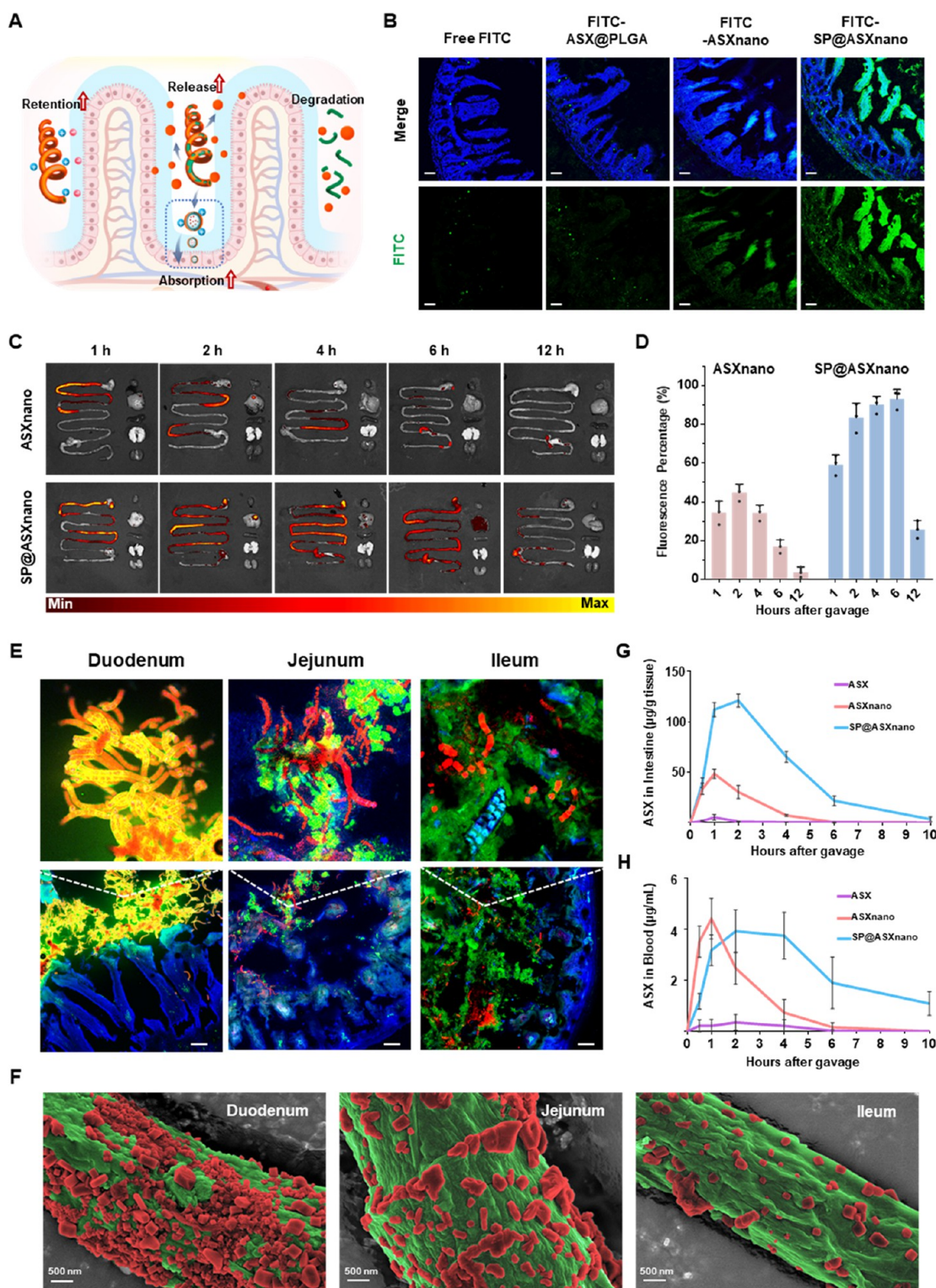


Figure 4. In vivo biodistribution. (A) Schematic illustration of the drug delivery of SP@ASXnano showing that microalgae SP and ASX nanoparticles have different features that complement each other. (B) Fluorescence images of the ileum at 4 h after the gavage of free FITC and FITC-labeled ASX@PLGA, ASXnano, and SP@ASXnano. Blue, DAPI; green, FITC. Scale bar, 50 μm . (C) Fluorescence images of ASXnano and SP@ASXnano in the gastrointestinal tract and main organs (top to bottom: heart, liver, spleen, lung, and kidney) at different time points after gavage. SP@ASXnano was imaged in the ASXnano channel. (D) The percentage of the materials' fluorescence area in the small intestinal area ($n = 3$). Data are presented as means + SD. (E) Fluorescence images of the small intestine (duodenum, jejunum, and ileum) at 4 h after the gavage of SP@ASXnano. Blue, DAPI; red, chlorophyll in SP; green, FITC in ASXnano. Scale bar, 100 μm . (F) SEM images (pseudocolor) of SP@ASXnano in the small intestine (duodenum, jejunum, and ileum) at 4 h after the gavage of SP@ASXnano. Scale bar, 500 nm. (G, H) Pharmacokinetic analysis of the ASX distribution in the mice's intestinal tissue (G) and blood (H) after the gavage of ASX, ASXnano, and SP@ASXnano, respectively ($n = 3$). Data are presented as means \pm SD. AUC in (G): ASX (9.1), ASXnano (114.5), SP@ASXnano (487.9); AUC in (H): ASX (1.3), ASXnano (10.8), SP@ASXnano (24.3).

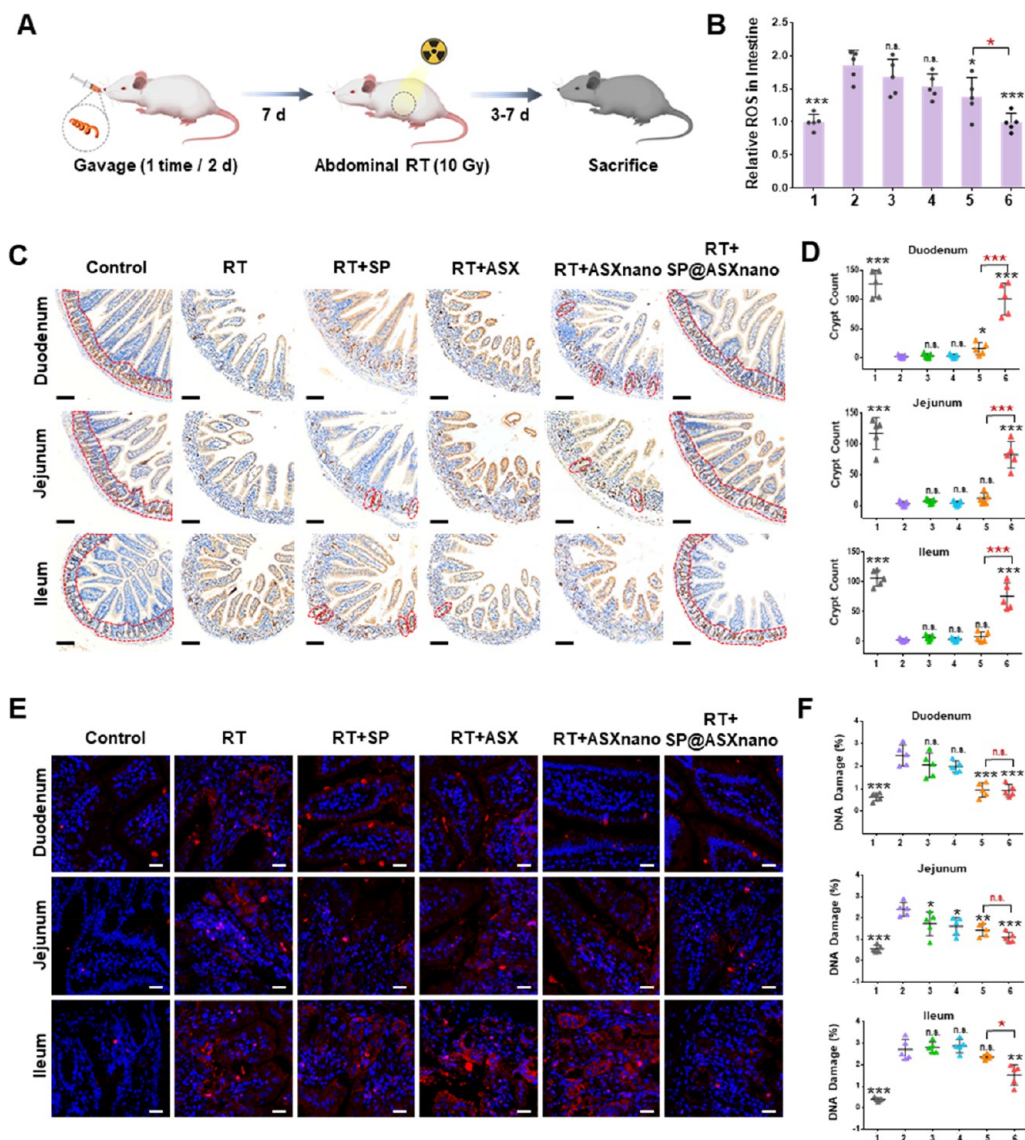


Figure 5. Protective effect against the intestinal injury induced by abdominal radiation. (A) Schematic illustration of the material administration, abdominal X-ray radiation (RT), and assessments. (B) The relative ROS levels in the small intestinal tissue of the mice after different treatments ($n = 5$). Treatments: 1, control; 2, RT; 3, RT+SP; 4, RT+ASX; 5, RT+ASXnano; 6, RT+SP@ASXnano. Results are presented as means \pm SD; black *, p vs RT group, red *, p between RT+ASXnano and RT+SP@ASXnano; *, $p < 0.05$, **, $p < 0.01$, ***, $p < 0.001$, n.s., no significance. (C, D) Regenerating crypts (brown, indicated with red dotted lines) in the small intestine (duodenum, jejunum, and ileum) (C) and the quantification ($n = 5$) (D). Scale bar, 100 μm . (E, F) Cellular DNA damage in the small intestine (E) and the quantification ($n = 5$) (F). Red fluorescence, DNA damage stained by γH2AX ; blue fluorescence, cell nuclei stained by DAPI. Scale bar, 25 μm . Results in (D) and (F) are presented as means \pm SD; black *, p vs RT group, red *, p between RT+ASXnano and RT+SP@ASXnano; *, $p < 0.05$, **, $p < 0.01$, ***, $p < 0.001$, n.s., no significance.

viability after the incubation with SP, ASX, ASXnano, and SP@ASXnano (Figure 3A). As shown in Figure 3B, the FITC-labeled ASXnano particles could be more effectively internalized over time compared with the ASX@PLGA nanoparticles, indicating that the positively charged CS coatings gave ASXnano superior cellular uptake. To evaluate the antioxidation in IEC-6 cells, the intracellular ROS production (green fluorescence) induced by 6 Gy of radiation (RT) was detected. As shown in Figure 3C,D, the RT-induced ROS generation was effectively reduced in the cells pretreated with ASX, ASXnano, and SP@ASXnano. However, the effect of SP treatment was not significant, indicating the antioxidant capacity of SP@ASXnano was mostly attributed to ASX but not SP. The colony formation ability of the irradiated cells also could be effectively protected by ASX,

ASXnano, and SP@ASXnano (Figure 3E,F). Figures S6–S9 showed the antioxidant and radioprotective effects of different materials in RAW264.7 (monocyte-macrophages) (Figures S6, S7) and LX-2 (hepatic stellate cells) (Figures S8, S9) through ROS and DNA double-strand break tests. These figures suggested that the pretreatment of SP@ASXnano could effectively reduce the cellular ROS generation and DNA damage induced by RT in these cell lines, thus having the potential to exert whole-body protection in vivo. And the effects of SP@ASXnano were better than ASXnano, ASX, and SP. Taken together, SP@ASXnano displayed high safety, notable antioxidant capacity, and cellular radioprotection in vitro.

In Vivo Biodistribution. As a microscale carrier with a spiral shape, SP was previously proved to have prolonged retention

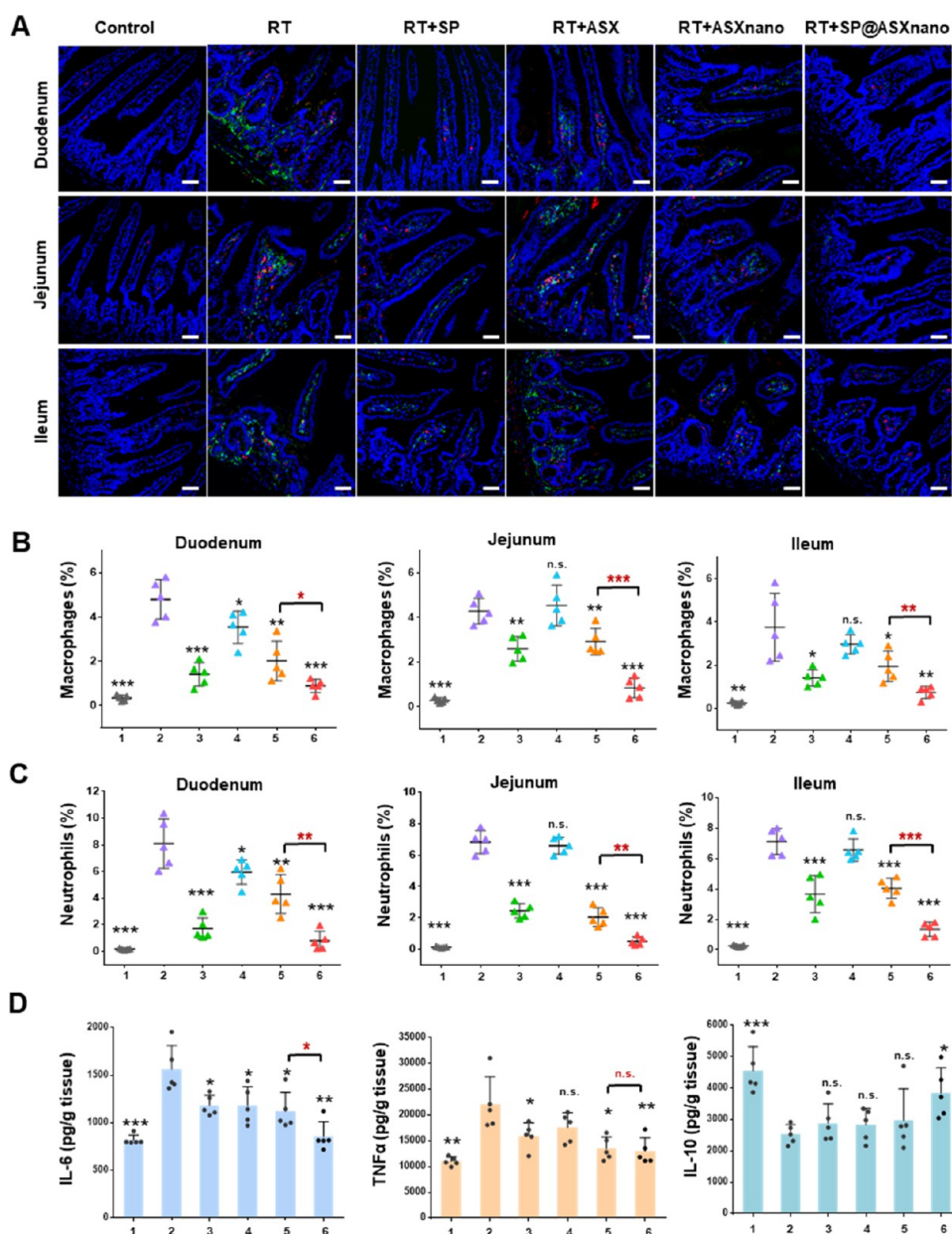


Figure 6. Protective effect against the intestinal injury induced by abdominal radiation. (A) Macrophages (green, stained by F4/80) and neutrophils (red, stained by Ly-6G) in the small intestine (duodenum, jejunum, and ileum). The cell nuclei were stained by DAPI (blue). Scale bar, 50 μm . (B, C) Quantification of macrophages (B) and neutrophils (C) ($n = 5$). Treatments: 1, control; 2, RT; 3, RT+SP; 4, RT+ASX; 5, RT+ASXnano; 6, RT+SP@ASXnano. Results are presented as means \pm SD. (D) The cytokines IL-6, TNF α , and IL-10 in the intestinal tissue ($n = 5$). Results are presented as means \pm SD. Black *, p vs RT group, red *, p between RT+ASXnano and RT+SP@ASXnano; *, $p < 0.05$, **, $p < 0.01$, ***, $p < 0.001$, n.s., no significance.

between intestinal villi.^{23,24} In this work, SP@ASXnano showed enhanced drug distribution in both the intestine and blood since microalgae SP and ASX nanoparticles showed different features that could complement each other. As shown in Figure 4A, SP provided prolonged intestinal retention, constant ASXnano release, and full degradation, while positively charged ASXnano enhanced intestinal absorption.

Compared with free FITC and FITC-labeled ASX@PLGA, the fluorescence of FITC-labeled ASXnano and SP@ASXnano in intestinal villi and submucosa was more significant in the duodenum (Figure S10), jejunum (Figure S11), and ileum (Figure 4B). This indicated that the encapsulation of the positively charged CS coatings and SP could effectively enhance

the intestinal penetration of the drug. Fluorescence imaging was used to detect the in vivo distribution of SP@ASXnano compared with ASXnano (Figure 4C,D) and SP (Figure S12), respectively. FITC was used to label ASXnano (Figure 4C,D), and the chlorophyll in SP was used to track SP (Figure S12). The distribution of ASXnano fluorescence was observed as shown in Figure 4C. The small intestine is the main position of drug absorption, and the large intestine has abundant microbiota.³⁵ Compared with free ASXnano particles, SP@ASXnano displayed longer retention and a larger coverage area over the whole small intestine (Figure 4D), indicating that the small intestinal distribution of ASXnano particles was improved by the loading of the SP, which could benefit the drug absorption into

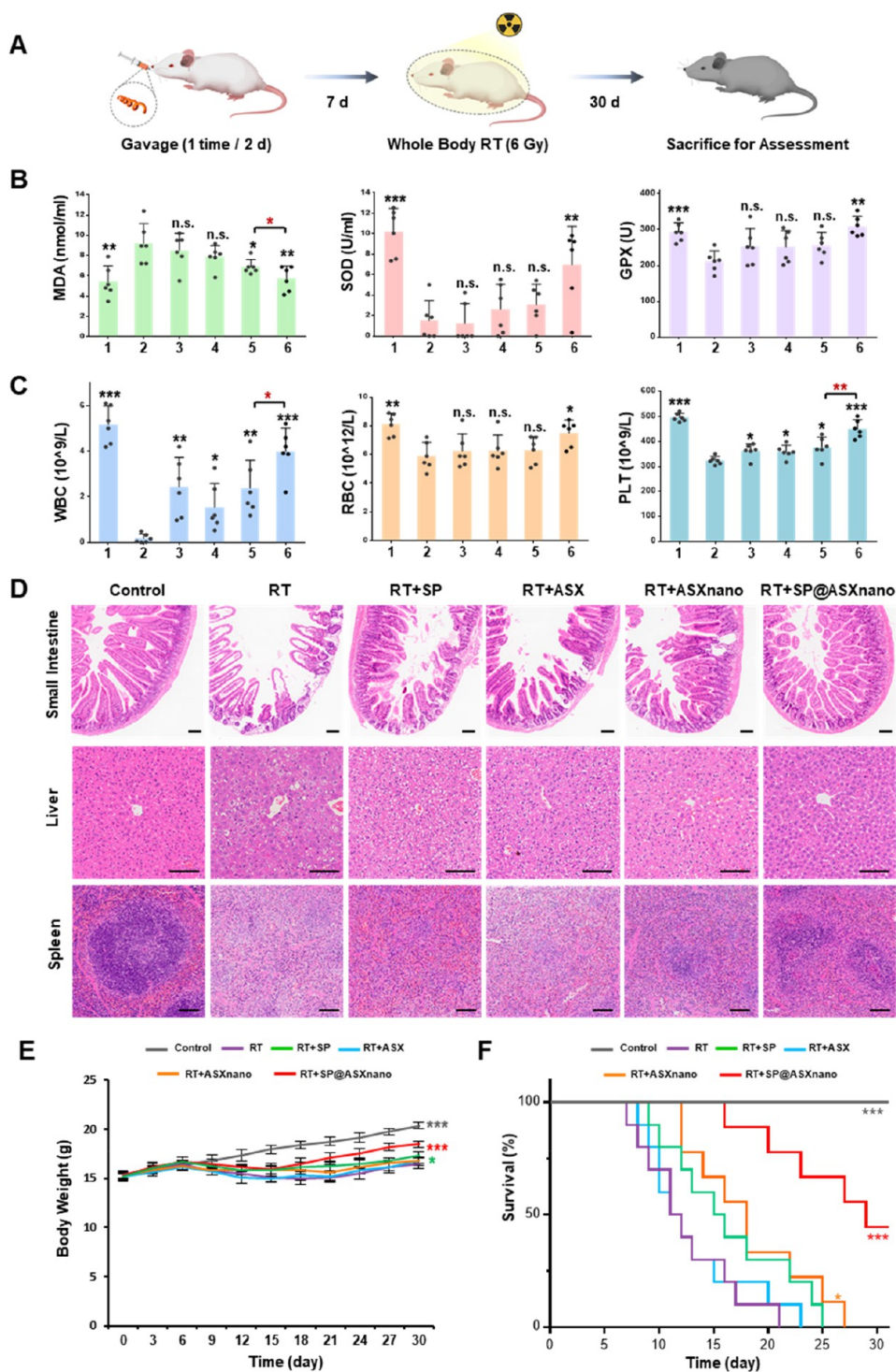


Figure 7. Protective effect against radiation-induced whole-body injury. (A) Schematic illustration of the material administration, whole-body X-ray radiation (RT), and assessments. (B) The concentration of malondialdehyde (MDA) and the activity of superoxide dismutase (SOD) and glutathione peroxidase (GPX) in the blood of mice after different treatments ($n = 6$). Treatments: 1, control; 2, RT; 3, RT+SP; 4, RT+ASX; 5, RT+ASXnano; 6, RT+SP@ASXnano. Results are presented as means + SD; black *, p vs RT group; red *, p between RT+ASXnano and RT+SP@ASXnano; *, $p < 0.05$, **, $p < 0.01$, ***, $p < 0.001$, n.s., no significance. (C) The levels of white blood cells (WBC), red blood cells (RBC), and blood platelets (PLT) of mice after different treatments ($n = 6$). Treatments: 1, control; 2, RT; 3, RT+SP; 4, RT+ASX; 5, RT+ASXnano; 6, RT+SP@ASXnano. Results are presented as means + SD; * $p < 0.05$, ** $p < 0.01$, *** $p < 0.001$, n.s., no significance. (D) Represented images of the small intestine (ileum), liver, and spleen in different groups. Scale bar = 100 μm . (E) Body weights of the mice in different groups ($n = 5$) after RT. Results are presented as means + SD; *, p vs RT group; *, $p < 0.05$, **, $p < 0.01$, ***, $p < 0.001$, n.s., no significance. (F) Survival curves of mice after being exposed to a fatal dose of whole-body RT (10 Gy) ($n = 10$).

the small intestine and blood. Besides, SP@ASXnano also exhibited prolonged and wider retention in the large intestinal

tract of mice, suggesting full contact with the microbiota in the large intestine for possible microbiota regulation. In the SP

channel, the distribution of SP@ASXnano was also superior to that of SP after 4 h (Figure S12), meaning that the ASXnano coating could enhance the retention of the SP in turn. This might be related to the mucoadhesive property of the ASXnano's chitosan coating because its positive charge could interact with the negatively charged mucins in the intestinal mucus as reported previously.^{36,37} Therefore, ASXnano and SP could improve the intestinal distribution of each other, which makes SP@ASXnano a rational and effective combination.

Furthermore, the SP@ASXnano in different sections of the small intestine was observed (Figures 4E, S7). The images in the SP channel (red) showed that considerable SP was retained on the intestinal surface and progressively degraded from the proximal small intestine (duodenum and jejunum) to the distal parts (ileum). The images in the ASXnano channel (green) displayed the significant distribution and absorption of ASXnano particles in intestinal villi and submucosa. Moreover, the magnified images presented a detachment of ASXnano particles from SP, in which their fluorescence showed colocalization in the duodenum and separated localization in the jejunum and ileum. This was further confirmed by the SEM images of SP@ASXnano in different intestinal parts (Figure 4F), indicating that SP@ASXnano could gradually release its surface ASXnano particles along the intestinal tract as a constant source of the drug.

To further evaluate the pharmacokinetic characteristics after the administration of SP@ASXnano, a liquid chromatography–mass spectrometry (LC-MS) test was applied to detect ASX in the small intestinal tissue and blood of mice (Figure 4G,H). The representative LC-MS chromatogram of ASX is shown in Figure S14. The solutions containing ASX and ASXnano (equivalent to SP@ASXnano) were given as comparisons. As shown in Figure 4G, the intestinal ASX concentration in the SP@ASXnano group was higher at all time points after gavage than that in the ASXnano group. In blood, although the drug concentration in the SP@ASXnano group was slightly lower at the first two time points compared with the ASXnano group, it kept higher afterward (Figure 4H). And the single use of ASX showed minimal drug distribution in both figures. Moreover, the area under the curve (AUC) value of the SP@ASXnano group in the intestine (Figure 4G) was over 4 times the value of the ASXnano group and over 40 times that of the ASX group. The AUC value of the SP@ASXnano group in the blood (Figure 4H) was over 2 times that of the ASXnano group and over 20 times that of the ASX group. At 4 h after gavage, the blood dose of the SP@ASXnano, ASXnano, and ASX groups was about 0.07%, 0.01%, and 0.004% of the gavage dose, respectively. These results suggested that ASXnano improved the ASX absorption and the SP further enhanced and prolonged its distribution in intestinal tissue and blood. The SP@ASXnano system exhibited significant distribution in the small intestine and increased drug concentration in the small intestine and blood, making it promising in small intestinal and systemic radioprotection. Besides, it also increased the distribution in the large intestine, which may benefit the gut microbiota and health in this site.

Protective Effect against Intestinal Radiation Injury.

To investigate the materials' protection against acute radiation enteritis, the mice were exposed to 10 Gy of abdominal RT after a week of the gavage treatment (Figure 5A). As shown in Figure 5B, the abdominal RT significantly increased the ROS generation in the small intestinal tissue. The administration of SP@ASXnano reduced the ROS level more effectively than ASXnano, whereas SP and ASX showed no significant effect.

The pathological examinations showed that the intestinal crypts were severely destroyed by RT and failed to regenerate (indicated by red dotted lines) (Figure 5C,D). The administration of SP@ASXnano effectively protected the regenerating cells in intestinal crypts of the duodenum, jejunum, and ileum. By contrast, the administration of ASXnano protected the crypts in the duodenum but not in the jejunum and ileum, indicating its limitation on distal intestinal protection. Likewise, the RT-induced DNA damage (red) in the ileum could only be prevented by SP@ASXnano, although that in the duodenum and jejunum could be reduced by both ASXnano and SP@ASXnano (Figure 5E,F).

The double immunofluorescent staining of the intestinal macrophages (green) and neutrophils (red) showed that the RT-induced inflammatory cells' infiltration was significantly inhibited by SP@ASXnano and moderately inhibited by ASXnano (Figure 6A–C). Besides, the usage of SP also decreased inflammatory cell infiltration, suggesting a synergy between SP and ASX. Moreover, RT caused the increase of pro-inflammatory cytokines (IL-6 and TNF- α) and the reduction of anti-inflammatory cytokine (IL-10) in the small intestinal tissue (Figure 6D). Compared with SP, ASX, and ASXnano, SP@ASXnano could best prevent this abnormality. To sum up, the oral administration of SP@ASXnano showed the most significant protection against radiation-induced intestinal injury.

Protective Effect against the Radiation-Induced Whole-Body Injury.

The radioprotective effect of SP@ASXnano on the whole body was evaluated (Figure 7A). The ROS generation induced by whole-body RT caused the increase of blood lipid peroxides, such as malondialdehyde (MDA), and the decrease of blood antioxidant enzymes, such as superoxide dismutase (SOD) and glutathione peroxidase (GPX) (Figure 7B). Significantly, the administration of SP@ASXnano and ASXnano reduced the blood MDA production and raised the blood SOD and GPX. As shown in Figure 7C, the whole-body RT caused damage to the hematopoietic function of bone marrow and led to the reduction of red blood cells (RBC), white blood cells (WBC), and blood platelets (PLT). SP@ASXnano could effectively maintain the levels of WBC, RBC, and PLT in the irradiated mice. The data in Figure 7B,C also showed the different degrees of protective effects provided by ASXnano, SP, and ASX, which were lower than the effect of SP@ASXnano however.

Furthermore, the pathological examination displayed that the use of SP@ASXnano alleviated the RT-induced histological abnormality in the radiosensitive organs (Figure 7D). Specifically, the integrity of the small intestinal epithelium was injured by RT. In the livers, enlarged intercellular spaces and extensive vacuolation were observed, indicating the hepatocytes' hydropic degeneration induced by RT. Moreover, RT caused a significant depletion of lymphocytes and an indistinct boundary between the white and red pulp in the spleens. Importantly, the histological structure of these organs could be almost entirely maintained by the gavage with SP@ASXnano, whereas the other treatments had no comparable effect. The records of the mice's body weights reflected the systemic damages resulting from the whole-body RT, in which the progressive emaciation was notably inhibited by SP@ASXnano and partly inhibited by SP (Figure 7E). The prevention of materials on the RT-induced death was tested under a fatal dose (10 Gy) of whole-body RT (Figure 7F). The median survival of the mice in the RT and RT + ASX groups was only 11.5 d. The SP@ASXnano treatment significantly increased the median survival to 29 d (*p*-value vs RT

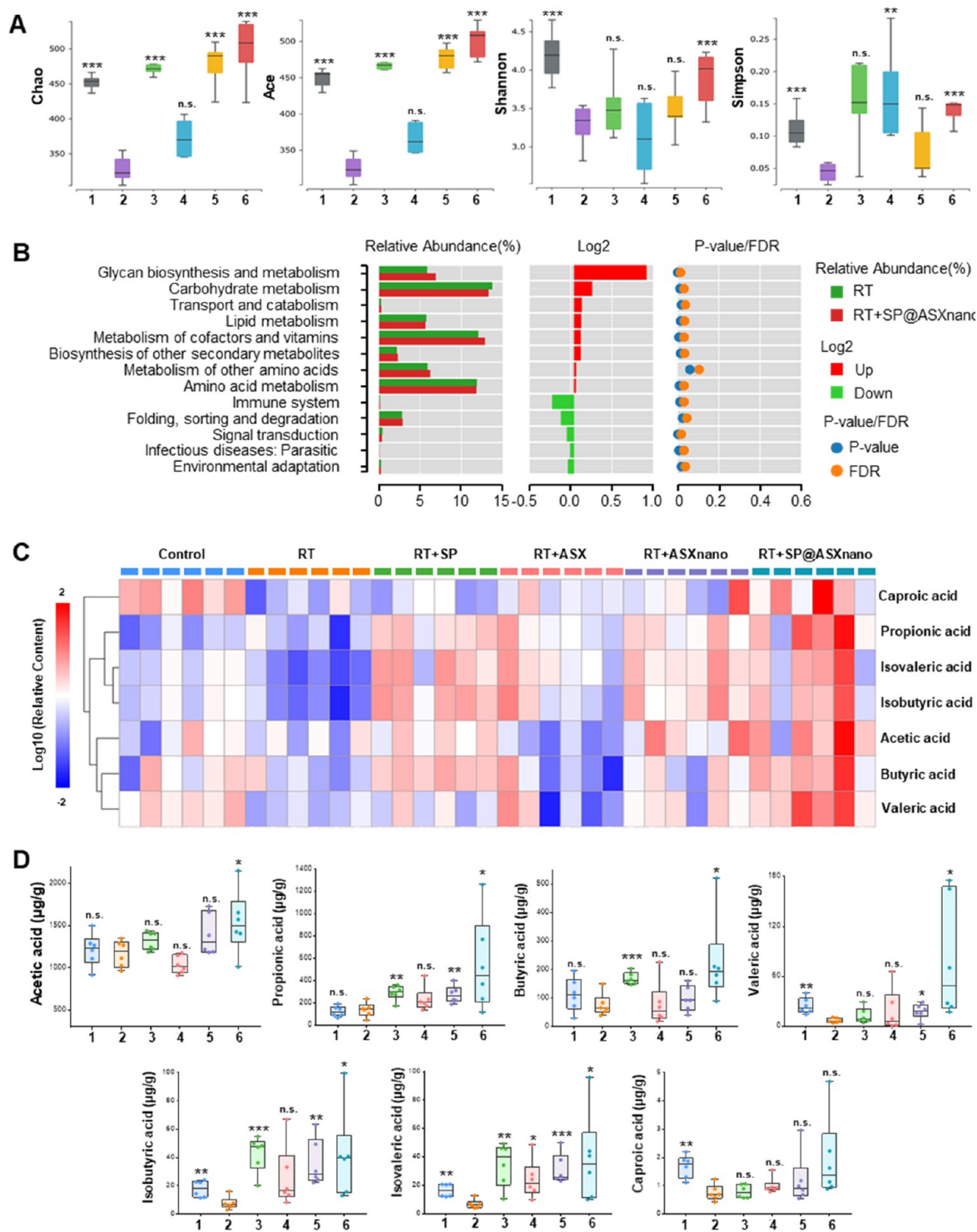


Figure 8. Effect on gut microbiota and fecal short-chain fatty acids (SCFAs). (A) Alpha diversity boxplots representing the microbiota community richness (Chao and Ace) and diversity (Shannon and Simpson) ($n = 8$). Treatments: 1, control; 2, RT; 3, RT+SP; 4, RT+ASX; 5, RT+ASXnano; 6, RT+SP@ASXnano. Results are presented as the boxes' bounds (the 25th to 75th percentile) and lines representing maxima, medians, and minima; *, p vs RT group; *, $p < 0.05$, **, $p < 0.01$, ***, $p < 0.001$, n.s., no significance. (B) The predicted differences in the KEGG (Kyoto Encyclopedia of Genes and Genomes) metabolic pathways between group RT and RT+SP@ASXnano. The left histogram, the relative abundance at the genus level; the middle histogram, the log2 values of the average relative abundance ratio; the right figure, the p values and FDR values obtained by the Wilcox test (p value and FDR value < 0.05 , representing significant difference). (C) Heat map of the relative content of seven fecal SCFAs in different groups. (D) Boxplot figure of seven fecal SCFAs' absolute content ($n = 6$). Results are presented as the boxes' bounds (the 25th to 75th percentile) and lines representing maxima, medians, and minima; *, p vs RT group; *, $p < 0.05$, **, $p < 0.01$, ***, $p < 0.001$, n.s., no significance.

group, < 0.001). The median survival was also prolonged by ASXnano (18 d) with statistical significance (p -value vs RT

group, < 0.05). The median survival in the SP group was mildly prolonged (15.5 d), but the difference between the RT group

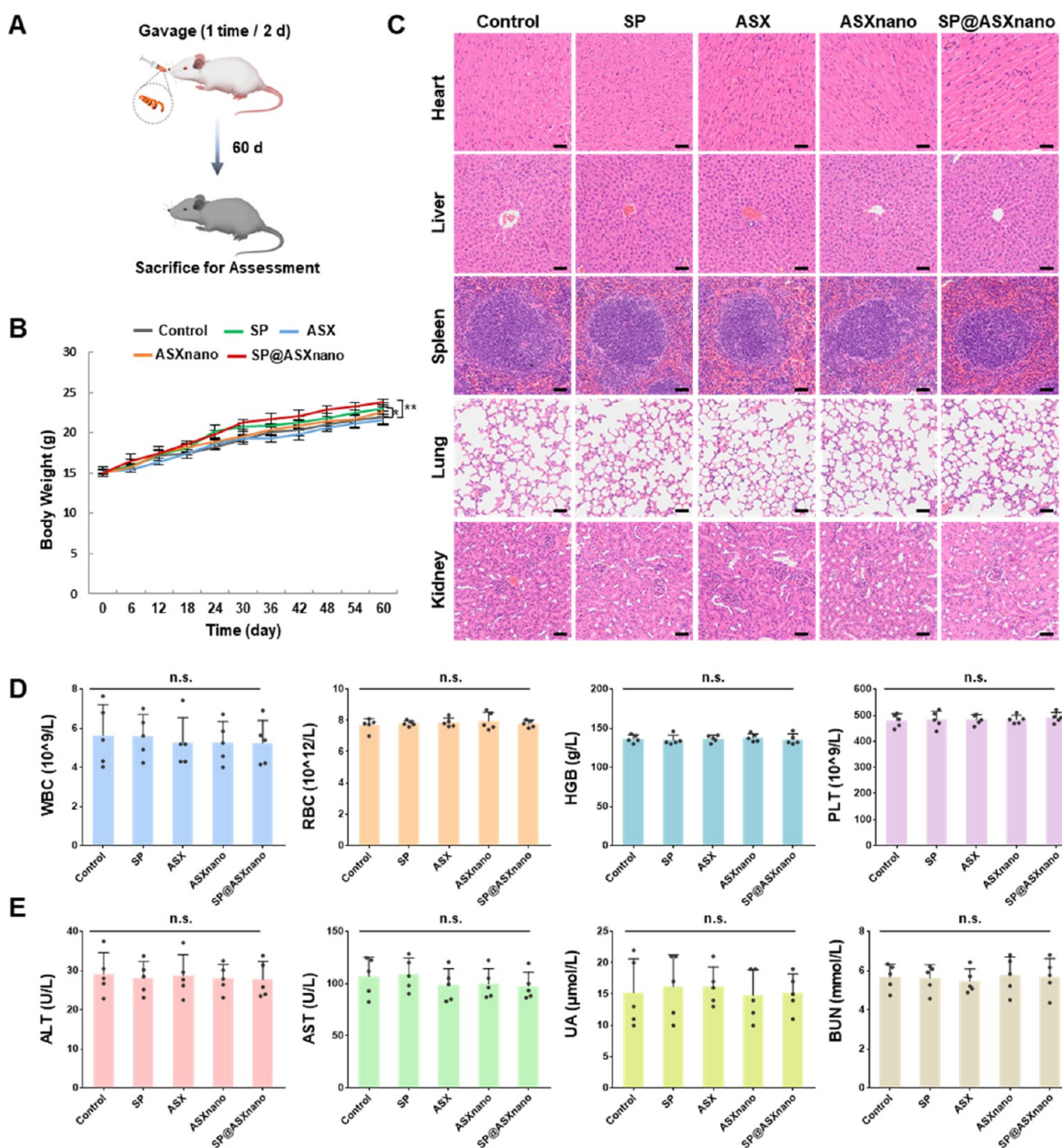


Figure 9. Long-term safety. (A) Schematic illustration of the material administration and assessments. (B) Body weight of the mice in different groups ($n = 5$). Results are presented as means \pm SD; *, p vs control group; *, $p < 0.05$, **, $p < 0.01$, ***, $p < 0.001$, n.s., no significance. (C) Representative HE images of the hearts, livers, spleens, lungs, and kidneys of the mice in different groups. Scale bar, 50 μm . (D–E) Hematological tests (D) and serum biochemical tests (E) of the mice. WBC, white blood cells; RBC, red blood cells; HGB, hemoglobin; PLT, blood platelet; ALT, alanine transferase; AST, aspartate transferase; UA, uric acid; BUN, blood urea nitrogen. Results are presented as means \pm SD; n.s., no significance.

was not statistically significant. These results illustrated the notable preventive effect of the SP@ASXnano on RT-induced systemic damage and even death.

Effect on Gut Microbiota and Fecal Short-Chain Fatty Acids. The functions of gut microbiota in gastrointestinal and host health have been widely studied.^{38,39} The bacteria in the colon can derive energy from the saccharolytic fermentation of nondigestible substrates and produce many nutrients and metabolites including SCFAs that can be absorbed into the bloodstream, thus reaching the whole-body tissue/organs.^{40–42} SCFA is an important link between intestinal microbiota and the host. For intestinal health, SCFAs can serve as an energy source for intestinal epithelial cells, which can participate in intestinal

mucosal immunity, inflammation, homeostasis, etc.^{43,44} For systemic health, SCFAs can bind to receptors in many tissue/organs and act as hormone signals thus influencing the physiology or diseases of the nervous, endocrine, immune, and cardiovascular systems.^{45–47} Importantly, the oral administration of ASX and SP has been reported to be beneficial to the gut microbiota composition and SCFAs production.^{23,29,31,48–51} Besides, the SP@ASXnano could be fully degraded in the intestine (Figure 3D). Therefore, we speculated that SP@ASXnano might be utilized by gut microbiota, therefore influencing its composition and the fecal SCFAs levels.

The 16S rRNA gene sequencing analysis revealed the richness (according to the index of Chao and Ace) and diversity

(according to the index of Shannon and Simpson) of gut microbiota between groups, which was displayed by the alpha diversity boxplots (Figure 8A). Specifically, both the richness and diversity of microbiota decreased after the whole-body RT. The oral administration of SP and ASXnano significantly raised the microbiota richness. And the richness and diversity of gut microbiota could be effectively increased by SP@ASXnano. Besides, the PLS-DA figure suggested the highest similarity of the RT+SP@ASXnano group's composition to normal mice compared with other RT groups, indicating that the SP@ASXnano administration could protect the microbiota composition against RT-induced damage (Figure S15). The separated use of SP, ASX, and ASXnano mildly changed the composition of irradiated microbiota, which is relatively inferior to the SP@ASXnano's effect, however.

As shown in Figure S16, the genus abundance distribution of the control group was significantly different from the RT group and the most similar to the RT+SP@ASXnano group, suggesting that the normal bacteria composition could be protected by SP@ASXnano treatment from the RT-induced changes. The difference between the RT group and the RT+SP@ASXnano group was analyzed. The genus that was significantly up/down-regulated in the RT+SP@ASXnano group (compared with the RT group, $p < 0.001$) was marked with red and green boxes, respectively. Among the up-regulated genus, *Clostridium IV* was reported with resistance to the invasion of outside microorganisms.⁵² *Mucispirillum* showed protection against colitis.⁵³ *Akkermansia* is a promising candidate for probiotics, which plays an important role in host metabolism, immunity, and antitumor effect.^{54,55} *Lactobacillus* and *Alloprevotella* could play beneficial roles in intestinal inflammatory diseases, with beneficial effects like producing SCFAs, reducing intestinal permeability, and the enhancing intestinal barrier.^{56–59} The up-regulation of these genera indicated the positive influence of SP@ASXnano treatment on the gut bacteria of RT mice. But the roles of several up-regulated genera (*Paraprevotella*, *Prevotella*, *Odoribacter*, *Alistipes*) and some down-regulated genera (*Saccharibacteria*, *Turicibacter*, *Butyrivibrio*) have not been clearly defined in this field. So, the meaning of these changes was also not clear, which should be deeply investigated in the future.

Furthermore, we analyzed the predicted differences between the RT and RT+SP@ASXnano groups in the Kyoto Encyclopedia of Genes and Genomes (KEGG) metabolic pathways (Figure 8B). The pathways linked to the metabolism of a series of main nutrients, such as carbohydrates, lipids, vitamins, and amino acids, were notably up-regulated by the administration of SP@ASXnano. The pathways related to the immune response, infection, environmental adaptation, etc., were decreased. However, other changes in pathways such as the down-regulation of the immune system were inexplicable and still should be further explored.

In addition, the levels of seven kinds of fecal SCFAs in different groups were detected. The relative content of SCFAs was shown as a heatmap (Figure 8C), and the absolute content was shown in Figure 8D. Compared with the untreated RT group, the administration of SP@ASXnano significantly increased the content of six fecal SCFAs except for caproic acid. The separated administration of SP and ASXnano respectively improved several (at most four) SCFAs' production at different levels, which suggested that the effect of SP@ASXnano could be the combination of SP and ASXnano. It has been reported that the intestinal SCFAs, especially the butyrate

acid, could act as the energy source and extracellular signaling molecules against RT-induced damage.⁶⁰ Accordingly, the radioprotective effect of SP@ASXnano might have been facilitated by its function on the SCFAs' regulation.

To sum up, the administration of SP@ASXnano displayed significant benefits on the gut microbiota and fecal SCFA levels of the irradiated mice, which should be a synergy between SP and ASXnano. This effect might contribute to the radioprotective effect of SP@ASXnano on the intestine and the whole body since the improvement of the gut microbiota and/or SCFAs has already been widely proven to be advantageous to the radiation-induced lesions.^{61–63} However, in-depth examinations are still required to illustrate the clear roles that SCFAs played in the radioprotective effect and disease development.

Long-Term Safety. To ensure long-term safety, the mice were orally administrated with different materials for 60 d (one time every 2 d) (Figure 9A). The blood, hearts, livers, spleens, lungs, and kidneys of the mice were harvested for assessment. The record of body weight showed that the administration of SP and SP@ASXnano significantly enhanced the weight gain, in which the effect of SP@ASXnano was stronger (Figure 9B). Since SP could fully degrade as shown in Figure 3 and has been proven rich in nutritional elements,²⁷ its benefit on weight gain should be rational. The HE-stained pathological sections displayed that SP, ASX, ASXnano, and SP@ASXnano did not harm the histological structure of the major organs (Figure 9C). Likewise, the hematological tests (Figure 9D) and serum biochemical tests (Figure 9E) did not show any toxicity of all materials on the blood cells and the function of the liver (represented by ALT and AST) and kidney (represented by UA and BUN). The results suggested the long-term safety of SP@ASXnano, which would be a prerequisite for its practical use against RT-induced injury.

Study Limitations. There were some limitations in this work. First, the significant radioprotective effect and fecal SCFAs' regulation of SP@ASXnano were revealed. But the clear roles that SCFAs played in the protective effect and disease development have not been deeply investigated. Second, the underlying mechanisms of some benefits of SP, such as the up-regulation of fecal SCFAs, are still not clear. Third, the potential of the system in other intestinal diseases has not been further investigated. Finally, the system's applicability to encapsulating other drugs still needs more testing and evaluation. These aspects should be important directions for future works.

CONCLUSIONS

In summary, we constructed an orally used microalgae-nano integrated system (SP@ASXnano) combined with microalgae SP and nanoparticles of ASX (ASXnano) for protection from radiation-induced intestinal and systemic injury. The advantages of SP@ASXnano in radiation-induced injury are mainly based on the intestinal delivery features of the microalgae-nano system and the actions of the cargo, ASX. The microalgae-nano system, as a drug carrier, provided an enhanced intestinal delivery. ASX is a powerful antioxidant with the advantage to clear radiation-induced free radicals and subsequent damages.

From another perspective, the integrated system fully took advantage of the complementation as well as synergy between SP and ASXnano. SP and ASXnano showed different delivery features which could complement each other to reach better drug distribution in both the intestine and blood, overcoming the low oral bioavailability of ASX. SP and ASXnano had many similar benefits which could form a synergy to get stronger

radioprotection. Therefore, this convenient and safe oral formulation has great potential in intestinal and systemic radioprotection. Furthermore, the synthesis strategy used the natural surface electronegativity of SP and facily reached a high loading efficiency without destroying the structures and bioactivities of SP and the drug. This system was expected as a versatile drug delivery platform to deliver other drugs because chitosan/PLGA nanoparticles have strong suitability for the encapsulation of many soluble/insoluble drugs. In this sense, it is hopeful to apply this system in the treatment of more diseases.

METHODS

Synthesis and Characterization of ASXnano. Chitosan-modified ASX@PLGA nanoparticles (ASXnano) were prepared as follows: (1) ASX were first loaded into PLGA nanoparticles with the classical O/W microemulsion method. Briefly, astaxanthin (10 mg, Energy Chemical) and poly(lactic-co-glycolic acid) (PLGA) (100 mg, Sigma-Aldrich) were dissolved in 2 mL of dichloromethane (DCM, Sinopharm Chemical Reagent Co., Ltd.). Then, 2% poly(vinyl alcohol) (PVA) (4 mL, MW: ~31 000, Sigma-Aldrich) aqueous solution was added to the mixture, and the emulsion was formed by a probe sonicator with an output power of 200 W for 5 min at 4 °C. The ASX@PLGA nanoparticles were initially formed after the volatilization of DCM by stirring for one night at room temperature. (2) Chitosan quaternary ammonium salt solution (10 mg/mL, 10 mL, Shanghai Macklin Biochemical Co., Ltd.) was added into the ASX@PLGA solution and stirred for 12 h at room temperature. After that, the ASXnano were collected after centrifugation (12 000 rpm, 15 min), washed with water to remove the unreacted reagents, and then stored as an aqueous solution at 4 °C for further experiments. For FITC (fluorescein isothiocyanate)-labeled ASXnano, the FITC powder (1 mg, Shanghai Aladdin Biochemical Technology Co., Ltd.) was dissolved into 0.1 mL of DMSO and then added into the ASX/PLGA mixture. Other synthetic procedures are the same as before. The nanostructural morphology of ASXnano was measured by transmission electron microscopy (TEM) (FEI Tecnai F20, USA) with the assistance of phosphotungstic acid staining. The changes in hydrodynamic size and zeta potential were recorded by a dynamic light scattering system (Malvern Panalytical Zetasizer Nano ZS90, UK). The optical spectra were acquired using a UV-vis-NIR spectrometer (Shimadzu UV-2600, Japan).

The EE of ASX in ASXnano was studied following a previously reported method with some modifications.⁶⁴ A series of known concentrations of ASX in an acetone/water mixture solution (1:2) were first measured to build a standard curve based on the absorbance peak at 475 nm through the UV-vis-NIR spectrometer. For the EE of ASX in ASXnano, the ASX was collected by hydrolyzing ASXnano, and then the concentration of ASX was determined by the absorbance at 475 nm.⁶⁵ The EE of ASX in ASXnano was over 95%. For the release behavior of ASX from ASXnano, 2 mL of ASXnano was added into a dialysis bag (MWCO = 300 kDa) and dialyzed in simulated gastric fluid (pH 1.2, 10 mL) at 37 °C for 1 h with gentle shaking and then transferred into 10 mL of simulated intestinal fluid (pH 7, 10 mL) for another 8 h. At different time points, the content of the released ASX in the medium was tested.

Synthesis and Characterization of SP@ASXnano. The cultured SP was collected and washed with phosphate-buffered saline (PBS) before use. SP (25 mg) was added to the PBS solution (50 mL) of ASXnano (1 mg of ASX). The mixture was softly shaken for 15 min. Afterward, the prepared SP@ASXnano was collected after centrifugation (4500 rpm, 10 min). The supernatant was also collected and measured for ASX concentration according to the standard curve. The EE was calculated by dividing the loaded amount of ASX by the total amount. To optimize EE, different weight ratios of SP/ASXnano (when the loading time was 15 min) and different loading times (when SP/ASXnano was 25) were tried. An optical microscope (Zeiss, Germany) and SEM microscopy (Hitachi SU-70, Japan) were used to study the morphology of SP and SP@ASXnano. The zeta potential of SP,

ASXnano, and SP@ASXnano was detected by a Malvern Zetasizer. The characteristic UV spectra of SP, ASXnano, and SP@ASXnano were measured from 200 to 800 nm. The prepared SP@ASXnano was dispersed into SGF and softly shaken for 1 h at 37 °C. Then, the SP@ASXnano was collected by centrifugation, transferred into SIF, and softly shaken for 4 h at 37 °C. The SGF-treated (1 h) and SIF-treated (2 and 4 h) SP@ASXnano were respectively collected and prepared for microscope and SEM observation. For the release behavior of ASXnano from SP@ASXnano, 2 mL of SP@ASXnano suspension was added into 10 mL of SGF at 37 °C for 1 h with gentle shaking and then transferred into 10 mL of SIF for another 8 h. At different time points, the supernatant fluid was collected after centrifugation and the concentration of ASX was tested.

In Vitro Experiments. Rat small intestinal epithelium cells (IEC-6 cells) (ATCC CRL-1592) were from EK-Bioscience, Shanghai. They were cultured in Dulbecco's modified Eagle medium (DMEM) supplemented with 10% fetal bovine serum (FBS), 1% antibiotics, and insulin (0.1 U/mL) at 37 °C with a 5% CO₂ atmosphere. For the toxicity test, IEC-6 cells were seeded in 96-well plates (1 × 10⁴ per well) and then incubated with different concentrations of SP@ASXnano/SP/ASX/ASXnano for 24 h. The concentrations of SP/ASX in the SP/ASX/ASXnano group were the same as that of the SP@ASXnano group. ASX was first dissolved by dimethyl sulfoxide (DMSO) before the preparation of the DMEM solution for later use. The cell viability (the ratio to the untreated cells) was measured with a standard methyl thiazolyl tetrazolium (MTT) assay kit (YEASEN, Shanghai, China). The FITC-labeled ASX@PLGA and ASXnano particles were applied to explore cell uptake over time. IEC-6 cells (1 × 10⁵) were seeded in confocal dishes (1 × 10⁵) overnight and then incubated with 1 mL of ASX@PLGA or ASXnano (5 μg ASX/mL) for 0, 1, 3, and 5 h. After incubation, the medium was removed. The cell nuclei and membrane were respectively stained by DAPI (blue) and Dil (red). To test the antioxidant effect of SP@ASXnano, IEC-6 cells were incubated with SP@ASXnano (5 μg ASX/mL) for 6 h. The cells in other treated groups were respectively incubated with SP, ASX, and ASXnano, which contained the same amount of SP/ASX. Afterward, the cells were washed and exposed to 6 Gy of X-ray (8.415 Gy/min) (X-RAD 160, Pxi, USA). A ROS kit (YEASEN, Shanghai, China) was used to stain the cellular ROS (green fluorescence). The ROS fluorescence area was analyzed using ImageJ software (1.8.0_112, National Institutes of Health, USA). The irradiated cells in the above groups were also seeded into six-well plates for the colony formation assay. After 5 days of culture, the cell colonies were fixed with methanol and stained with a crystal violet solution (purple) for counting the surviving colonies (with more than 50 cells). Surviving fraction was the percentage of the colony counts in the seeded cells. To evaluate the in vitro antioxidant and radioprotective effect of SP@ASXnano in the whole body, RAW264.7 (mouse leukemia cells of monocyte-macrophage) and LX-2 (human hepatic stellate cells) were used for the tests of radiation-induced ROS generation and DNA damage. The pretreatments with different materials and the X-ray radiation followed the same protocols of the tests carried out in the IEC-6 cells. After radiation, the cells were respectively stained with the ROS kit (probe, DCFH-DA) and DNA double-strand break kit (marker, γH2AX) following the instructions.

In Vivo Biodistribution. All animal studies were approved by the Institutional Animal Care and Use Committee of Zhejiang University (AIRB-2021-952) and performed according to the National Institute of Health Guide for the Care and Use of Laboratory Animals.

To observe the materials' penetration in the intestinal tissue, the mice's ileum was collected at about 4 h after gavage of free FITC and FITC-labeled ASX@PLGA, ASXnano, and SP@ASXnano. The tissue was washed, sectioned, and stained with DAPI for fluorescence observation. To visualize the distribution of SP and FITC-labeled ASXnano and SP@ASXnano in the intestine and other organs, the in vivo fluorescence imaging was detected using an IVIS Lumina LT Series III (PerkinElmer, USA). The FITC channel (Ex: 445–490 nm, Em: 515–575 nm) was used to detect the fluorescence of ASXnano and SP@ASXnano. And the chlorophyll fluorescence of SP (Ex: 605 nm, Em: 615–665 nm) was used to detect the fluorescence of SP and SP@ASXnano. In detail, Balb/c mice (6 weeks, female) were given the water

solution of SP, ASXnano, and SP@ASXnano, respectively, after 12 h of fasting. After 1, 2, 4, 6, and 12 h, the mice's gastrointestinal tracts, hearts, livers, spleens, lungs, and kidneys were collected and imaged to detect the fluorescence of SP (chlorophyll) and ASXnano (FITC), respectively. The fluorescence area (%) of materials was calculated as its proportion of the whole small intestinal area, which was analyzed by Living Image 4.5 software (PerkinElmer, USA). For the observation of FITC-labeled SP@ASXnano in intestinal tissue, the mice's small intestine (duodenum, jejunum, and ileum) and contents were collected at about 4 h after gavage. The tissue was washed, sectioned, and stained with DAPI for fluorescence observation. The intestinal contents were prepared for SEM observation. LC-MS analysis was used to detect ASX concentration in intestinal tissue and blood after gavage for the pharmacokinetic study. Balb/c mice (6 weeks, female) were fasted for 12 h and given the water solution of ASX, ASXnano, and SP@ASXnano at the dose of 50 mg ASX/kg (gavage volume, 500 μ L), respectively. ASX was also first dissolved by DMSO at a high concentration and then diluted by water at a 1:10 ratio to prepare the ASX solution. At different time points, the small intestine and blood were collected and prepared into homogenate and serum, respectively. The samples were vortex-mixed with methyl *tert*-butyl ether (v:v = 1:2) for 10 min and then centrifuged for 10 min at the speed of 4500g. The upper layer of the solution was transferred into a new tube and dried by nitrogen flow. The residual extract was reconstituted with methanol for LC-MS analysis. LC-MS instruments and conditions with detail are provided in the [Supporting Information](#).

Protective Effect against the Radiation-Induced Intestinal Injury. To evaluate the prevention of SP@ASXnano against radiation-induced intestinal injury, 6-week-old female Balb/c mice were orally administered water solutions of SP@ASXnano (50 ASX mg/kg, volume 500 μ L, once every 2 d) for 1 week. Afterward, the mice's abdomen area (up to the diaphragm, down to the pelvis) was exposed to 10 Gy of X-ray. The mice in other groups were given equivalent SP, ASX, and ASXnano solutions as treated comparisons. Normal mice without RT and the irradiated mice without treatments were set as control groups.

After RT, the small intestinal tissue of mice was immediately collected and prepared into a homogenate for the ROS measurement following the instructions of the tissue ROS test kit (DHE) (Biorab). The relative intestinal ROS was calculated as the intensity ratios of the RT groups to the normal group. Some small intestinal tissue was prepared for the pathological examination to detect cellular DNA damage (stained by γ H2AX, red fluorescence). Three days after RT, the small intestinal tissue was collected and prepared for the pathological immunohistochemistry (IHC) examination to detect the regenerating crypts (stained by Ki67, DAB). A week after RT, the small intestinal tissue was collected for immunofluorescent (IF) staining. The intestinal macrophages and neutrophils were respectively stained by F4/80 (green fluorescence) and Ly-6G (red fluorescence) using double-fluorescence staining. The cell nuclei were stained by DAPI (blue fluorescence). The number of Ki67-stained intestinal crypts in a cross-section was scored. The relative fluorescence area of the γ H2AX⁺ cells, macrophages, and neutrophils was measured. Enzyme-linked immunoabsorbent assay (ELISA) kits (RayBiotech) were applied to detect two pro-inflammatory cytokines (IL-6 and TNF- α) and one anti-inflammatory cytokine (IL-10) in the small intestinal tissue.

Protective Effect against the Radiation-Induced Whole-Body Injury. To evaluate the radioprotective effect of SP@ASXnano on the whole body, 6-week-old female Balb/c mice were orally administered a water solution of SP@ASXnano (50 ASX mg/kg, once every 2 d) for 1 week. Afterward, the mice were exposed to 6 Gy of whole-body RT. The body weights of mice were monitored for 30 d after RT, and the mice were then euthanized for assessments. The blood was collected for the routine examination and MDA, SOD, and GPX. The small intestine, livers, and spleens of mice were collected for pathological examination. To assess the materials' protective effect from the whole-body radiation-induced death, the mice were exposed to a fatal dose of whole-body X-ray radiation (10 Gy). The administration of different materials followed the mentioned procedures, and the survival time of mice was recorded for 30 d after RT.

Effect on Gut Microbiota and Fecal Short-Chain Fatty Acids.

The effect of materials on the irradiated gut microbiota was tested through 16S rRNA gene sequencing and analysis (BGI Co., Ltd.). Six-week-old female Balb/c mice were orally given different materials for 1 week and exposed to whole-body RT as described before. After another 30 d of treatments, the mice's feces were collected for gene sequencing. The samples with the successfully constructed libraries were analyzed. The DNA extraction and library construction followed the protocols previously used.²³ Some of the mice's feces were collected for the analysis of seven kinds of SCFAs (acetic acid, propionic acid, isobutyric acid, butyric acid, isovaleric acid, valeric acid, and caproic acid) (BioNovoGene Co., Ltd.). The sample preparation and the conditions of gas chromatography and mass spectra followed the protocols in the previous study.^{66–68}

Long-Term Safety. To assess the long-term safety, 6-week-old female Balb/c mice were orally given SP@ASXnano (50 ASX mg/kg, once every 2 d) for 60 days. The mice in other groups were given equivalent SP, ASX, and ASXnano solutions as comparisons. The mice's body weights were recorded during this period. Afterward, the mice were euthanized, and their blood, hearts, livers, spleens, lungs, and kidneys were collected for hematological and pathological examinations.

Statistical Analysis. The results from at least three independent experiments were presented as mean \pm standard deviation (SD). The difference between the data of any two groups was calculated by the two-tailed Student's *t* test. The statistical significance was indicated as *, $p < 0.05$; **, $p < 0.01$; ***, $p < 0.001$; n.s., no significance. All statistical analyses were performed by GraphPad Prism v.7.00 (GraphPad Software).

ASSOCIATED CONTENT

Supporting Information

The Supporting Information is available free of charge at <https://pubs.acs.org/doi/10.1021/acsnano.3c01502>.

Additional data, including supplementary methods, the zeta potential of ASX@PLGA and ASXnano particles, the original SEM images of [Figure 2F](#), encapsulation efficiency under different loading times, the original SEM images of [Figure 2J](#) and [Figure 4E](#), the ROS generation and cellular DNA damage of RAW264.7 cells and LX-2 cells, fluorescence images of the duodenum and jejunum after the gavage of free FITC and FITC-labeled ASX@PLGA, ASXnano, and SP@ASXnano, fluorescence images of SP and SP@ASXnano in the gastrointestinal tract and main organs, fluorescence images with split channels of the small intestine after the gavage of SP@ASXnano, representative LC-MS chromatogram of ASX, beta diversity PLS-DA (partial least-squares discrimination analysis) figure, and heatmap of the gut bacteria in different groups at the genus level ([PDF](#))

AUTHOR INFORMATION

Corresponding Authors

Min Zhou – Department of Surgery, The Fourth Affiliated Hospital, Zhejiang University School of Medicine, Yiwu 322000, China; Zhejiang University-University of Edinburgh Institute (ZJU-UoE Institute), Zhejiang University School of Medicine, Zhejiang University, Haining 314400, China; Institute of Translational Medicine, Zhejiang University, Hangzhou 310009, China; Cancer Center, Zhejiang University, Hangzhou 310058, China; Research Center for Life Science and Human Health, Binjiang Institute of Zhejiang University, Hangzhou 310053, China; orcid.org/0000-0002-7319-9570; Email: zhoum@zju.edu.cn

Hongyu Yu – Department of Gastroenterology, Shanghai East Hospital, Tongji University School of Medicine, Shanghai 200120, China; Email: yuhongyu1962@163.com

Zhe Tang – Department of Surgery, The Fourth Affiliated Hospital, Zhejiang University School of Medicine, Yiwu 322000, China; Email: 8xi@zju.edu.cn

Authors

Dongxiao Zhang – Department of Surgery, The Fourth Affiliated Hospital, Zhejiang University School of Medicine, Yiwu 322000, China; Zhejiang University-University of Edinburgh Institute (ZJU-UoE Institute), Zhejiang University School of Medicine, Zhejiang University, Haining 314400, China; Institute of Translational Medicine, Zhejiang University, Hangzhou 310009, China

Jian He – Department of Surgery, The Fourth Affiliated Hospital, Zhejiang University School of Medicine, Yiwu 322000, China; Zhejiang University-University of Edinburgh Institute (ZJU-UoE Institute), Zhejiang University School of Medicine, Zhejiang University, Haining 314400, China; Institute of Translational Medicine, Zhejiang University, Hangzhou 310009, China

Jiarong Cui – Institute of Translational Medicine, Zhejiang University, Hangzhou 310009, China

Ruoxi Wang – Institute of Translational Medicine, Zhejiang University, Hangzhou 310009, China

Complete contact information is available at:

<https://pubs.acs.org/10.1021/acsnano.3c01502>

Author Contributions

D.Z. and J.H. contributed equally to this work and carried out the experiments, data analysis, and manuscript writing. J.C. and R.W. contributed to the data analysis, figure layout, and writing. M.Z., Z.T., and H.Y. designed and directed the research and revised the manuscript.

Notes

The authors declare no competing financial interest.

ACKNOWLEDGMENTS

This work was supported by the National Key R&D Program of China (No. 2022YFA1104900), the National Natural Science Foundation of China (NSFC, No. 81971667 and 81870418), Binjiang Institute of Zhejiang University (ZY202205SMKY007), and the Key Research and Development Project of Zhejiang Province (No. 2020C03035). We gratefully acknowledge the Core Facility of Zhejiang University School of Medicine for the technical support. We thank the technical support by the Core Facility, Zhejiang University–University of Edinburgh Institute.

REFERENCES

- (1) Mettler, F. A.; Voelz, G. L. Major Radiation Exposure — What to Expect and How to Respond. *Engl. J. Med.* **2002**, *346*, 1554–1561.
- (2) Kathren, R. L. Radiation protection. *Science* **1967**, *156*, 544–550.
- (3) De Ruyscher, D.; Niedermann, G.; Burnet, N. G.; Siva, S.; Lee, A. W. M.; Hegi-Johnson, F. Radiotherapy toxicity. *Nat. Rev. Dis. Primers* **2019**, *5*, 13.
- (4) Chandra, R. A.; Keane, F. K.; Voncken, F.; Thomas, C. R. Contemporary radiotherapy: present and future. *Lancet* **2021**, *398*, 171–184.
- (5) Loge, L.; Florescu, C.; Alves, A.; Menahem, B. Radiation enteritis: Diagnostic and therapeutic issues. *J. Visc. Surg.* **2020**, *157*, 475–485.
- (6) Obrador, E.; Salvador, R.; Villascusa, J. I.; Soriano, J. M.; Estrela, J. M.; Montoro, A. Radioprotection and Radiomitigation: From the Bench to Clinical Practice. *Biomedicines* **2020**, *8*, 461.
- (7) Roberts, G. C.; Kelly, G. N. Radiation protection standards. *Lancet* **1993**, *341*, 1146–1147.
- (8) Azzam, E. I.; Jay-Gerin, J. P.; Pain, D. Ionizing radiation-induced metabolic oxidative stress and prolonged cell injury. *Cancer Lett.* **2012**, *327*, 48–60.
- (9) Stratford, M.; Hodgkiss, R. J.; Watfa, R. R. Studies on the role of antioxidants in radioprotection. *Pharmacol. Ther.* **2006**, *79*, 2194–2201.
- (10) Kumar, S.; Kumar, R.; Kumari, A.; Panwar, A. Astaxanthin: A super antioxidant from microalgae and its therapeutic potential. *J. Basic Microbiol.* **2022**, *62*, 1064–1082.
- (11) Kurinnyi, D. A.; Rushkovsky, S. R.; Dybska, O. B.; Dubrovina, G. V.; Pilinska, M. A. Astaxanthin modifies clastogenic effects of ionizing radiation in vitro in peripheral blood lymphocytes of the persons recovered from acute radiation sickness. *Exp. Oncol.* **2016**, *38*, 280–282.
- (12) Pilinska, M. A.; Kurinnyi, D. A.; Rushkovsky, S. R.; Dybska, O. B. Genoprotective properties of astaxanthin revealed by ionizing radiation exposure in vitro on human peripheral blood lymphocytes. *Probl. Radiac. Med. Radiobiol.* **2016**, *21*, 141–148.
- (13) Xue, X. L.; Han, X. D.; Li, Y.; Chu, X. F.; Miao, W. M.; Zhang, J. L.; Fan, S. J. Astaxanthin attenuates total body irradiation-induced hematopoietic system injury in mice via inhibition of oxidative stress and apoptosis. *Stem Cell Res. Ther.* **2017**, *8*, 7.
- (14) Donoso, A.; González, J.; Muoz, A. A.; González, P.; Agurto-Muoz, C. "Therapeutic uses of natural astaxanthin: An evidence-based review focused on human clinical trials". *Pharmacol. Res.* **2021**, *166*, 105479.
- (15) Fakhri, S.; Abbaszadeh, F.; Dargahi, L.; Jorjani, M. Astaxanthin: A mechanistic review on its biological activities and health benefits. *Pharmacol. Res.* **2018**, *136*, 1–20.
- (16) Martínez-Alvarez, O.; Calvo, M. M.; Gómez-Estaca, J. Recent Advances in Astaxanthin Micro/Nanoencapsulation to Improve Its Stability and Functionality as a Food Ingredient. *Mar. Drugs* **2020**, *18*, 406.
- (17) Chen, Z.; Li, W.; Shi, L.; Jiang, L.; Li, M.; Zhang, C.; Peng, H. Kidney-targeted astaxanthin natural antioxidant nanosystem for diabetic nephropathy therapy. *Eur. J. Pharm. Biopharm.* **2020**, *156*, 143–154.
- (18) Liu, C.; Zhang, S.; McClements, D. J.; Wang, D.; Xu, Y. Design of Astaxanthin-Loaded Core-Shell Nanoparticles Consisting of Chitosan Oligosaccharides and Poly(lactic-co-glycolic acid): Enhancement of Water Solubility, Stability, and Bioavailability. *J. Agric. Food Chem.* **2019**, *67*, 5113–5121.
- (19) Yang, L.; Li, F.; Cao, X.; Qiao, X.; Xue, C.; Xu, J. Stability and bioavailability of protein matrix-encapsulated astaxanthin ester microcapsules. *J. Sci. Food Agric.* **2022**, *102*, 2144–2152.
- (20) Zaroni, F.; Vakarelova, M.; Zoccatelli, G. Development and Characterization of Astaxanthin-Containing Whey Protein-Based Nanoparticles. *Mar. Drugs* **2019**, *17*, 627.
- (21) Zhu, Y.; Gu, Z.; Liao, Y.; Li, S.; Xue, Y.; Firempong, M. A.; Xu, Y.; Yu, J.; Smyth, H. D.; Xu, X. Improved intestinal absorption and oral bioavailability of astaxanthin using poly(ethylene glycol)-graft-chitosan nanoparticles: preparation, in vitro evaluation, and pharmacokinetics in rats. *J. Sci. Food Agric.* **2022**, *102*, 1002–1011.
- (22) Yang, J.; Zhou, Q.; Huang, Z.; Gu, Z.; Cheng, L.; Qiu, L.; Hong, Y. Mechanisms of in vitro controlled release of astaxanthin from starch-based double emulsion carriers. *Food Hydrocoll.* **2021**, *119*, 106837.
- (23) Zhang, D.; Zhong, D.; Ouyang, J.; He, J.; Qi, Y.; Chen, W.; Zhang, X.; Tao, W.; Zhou, M. Microalgae-based oral microcarriers for gut microbiota homeostasis and intestinal protection in cancer radiotherapy. *Nat. Commun.* **2022**, *13*, 1413.
- (24) Zhong, D.; Zhang, D.; Chen, W.; He, J.; Ren, C.; Zhang, X.; Kong, N.; Tao, W.; Zhou, M. Orally deliverable strategy based on microalgal biomass for intestinal disease treatment. *Sci. Adv.* **2021**, *7*, 48.

- (25) Zhong, D.; Zhang, D.; Xie, T.; Zhou, M. Biodegradable Microalgae-Based Carriers for Targeted Delivery and Imaging-Guided Therapy toward Lung Metastasis of Breast Cancer. *Small* **2020**, *16*, 20.
- (26) Zhong, D.; Li, W.; Qi, Y.; He, J.; Zhou, M. Photosynthetic Biohybrid Nanoswimmers System to Alleviate Tumor Hypoxia for FL/PA/MR Imaging-Guided Enhanced Radio-Photodynamic Synergetic Therapy. *Adv. Funct. Mater.* **2020**, *30*, 17.
- (27) Torres-Tiji, Y.; Fields, F. J.; Mayfield, S. P. Microalgae as a future food source. *Biotechnol. Adv.* **2020**, *41*, 107536.
- (28) Wu, Q.; Liu, M.; Miron, A.; Klímová, B.; Wan, D.; Kuca, K. The antioxidant, immunomodulatory, and anti-inflammatory activities of Spirulina: an overview. *Arch. Toxicol.* **2016**, *90*, 1817–1840.
- (29) Yu, T.; Wang, Y.; Chen, X.; Xiong, W.; Tang, Y.; Lin, L. Spirulina platensis alleviates chronic inflammation with modulation of gut microbiota and intestinal permeability in rats fed a high-fat diet. *J. Cell Mol. Med.* **2020**, *24*, 8603–8613.
- (30) Hu, J.; Li, Y.; Pakpour, S.; Wang, S.; Pan, Z.; Liu, J.; Wei, Q.; She, J.; Cang, H.; Zhang, R. X. Dose Effects of Orally Administered Spirulina Suspension on Colonic Microbiota in Healthy Mice. *Front. Cell Infect. Microbiol.* **2019**, *9*, 243.
- (31) Li, T. T.; Huang, Z. R.; Jia, R. B.; Lv, X. C.; Zhao, C.; Liu, B. Spirulina platensis polysaccharides attenuate lipid and carbohydrate metabolism disorder in high-sucrose and high-fat diet-fed rats in association with intestinal microbiota. *Food Res. Int.* **2021**, *147*, 110530.
- (32) Fabiano, A.; Beconcini, D.; Migone, C.; Piras, A. M.; Zambito, Y. Quaternary Ammonium Chitosans: The Importance of the Positive Fixed Charge of the Drug Delivery Systems. *Int. J. Mol. Sci.* **2020**, *21*, 18.
- (33) Lin, Y. H.; Sonaje, K.; Lin, K. M.; Juang, J. H.; Mi, F. L.; Yang, H. W.; Sung, H. W. Multi-ion-crosslinked nanoparticles with pH-responsive characteristics for oral delivery of protein drugs. *J. Controlled Release* **2008**, *132*, 141–149.
- (34) Motiei, M.; Kashanian, S. Novel amphiphilic chitosan nano-carriers for sustained oral delivery of hydrophobic drugs. *Eur. J. Pharm. Sci.* **2017**, *99*, 285–291.
- (35) Tropini, C.; Earle, K. A.; Huang, K. C.; Sonnenburg, J. L. The Gut Microbiome: Connecting Spatial Organization to Function. *Cell Host Microbe* **2017**, *21*, 433–442.
- (36) Mohammed, M. A.; Syeda, J. T. M.; Wasan, K. M.; Wasan, E. K. An Overview of Chitosan Nanoparticles and Its Application in Non-Parenteral Drug Delivery. *Pharmaceutics* **2017**, *9*, 4.
- (37) Pathomthongtaweetchai, N.; Muanprasat, C. Potential Applications of Chitosan-Based Nanomaterials to Surpass the Gastrointestinal Physiological Obstacles and Enhance the Intestinal Drug Absorption. *Pharmaceutics* **2021**, *13*, 6.
- (38) Robles Alonso, V.; Guarner, F. Linking the gut microbiota to human health. *Br. J. Nutr.* **2013**, *109*, S21–26.
- (39) Hou, K.; Wu, Z. X.; Chen, X. Y.; Wang, J. Q.; Zhang, D.; Xiao, C.; Zhu, D.; Koya, J. B.; Wei, L.; Li, J.; Chen, Z. S. Microbiota in health and diseases. *Signal Transduct. Target. Ther.* **2022**, *7*, 135.
- (40) McNeil, N. I.; Cummings, J. H.; James, W. P. Short chain fatty acid absorption by the human large intestine. *Gut* **1978**, *19*, 819–822.
- (41) Sellin, J. H.; DeSoignie, R. Short-chain fatty acid absorption in rabbit colon in vitro. *Gastroenterology* **1990**, *99*, 676–683.
- (42) Duca, F. A.; Lam, T. K. Gut microbiota, nutrient sensing and energy balance. *Diabetes Obes. Metab.* **2014**, *16*, 68–76.
- (43) Martin-Gallausiaux, C.; Marinelli, L.; Blottière, H. M.; Larraufie, P.; Lapaque, N. SCFA: mechanisms and functional importance in the gut. *Proc. Nutr. Soc.* **2021**, *80*, 37–49.
- (44) Sanderson, I. R. Short chain fatty acid regulation of signaling genes expressed by the intestinal epithelium. *J. Nutr.* **2004**, *134*, 2450–2454.
- (45) Kimura, I.; Ichimura, A.; Ohue-Kitano, R.; Igarashi, M. Free Fatty Acid Receptors in Health and Disease. *Physiol. Rev.* **2020**, *100*, 171–210.
- (46) Tolhurst, G.; Heffron, H.; Lam, Y. S.; Parker, H. E.; Habib, A. M.; Diakogiannaki, E.; Cameron, J.; Grosse, J.; Reimann, F.; Gribble, F. M. Short-chain fatty acids stimulate glucagon-like peptide-1 secretion via the G-protein-coupled receptor FFAR2. *Diabetes* **2012**, *61*, 364–371.
- (47) Lymperopoulos, A.; Suster, M. S.; Borges, J. I. Short-Chain Fatty Acid Receptors and Cardiovascular Function. *Int. J. Mol. Sci.* **2022**, *23*, 3033.
- (48) Wu, L.; Lyu, Y.; Srinivasagan, R.; Wu, J.; Ojo, B.; Tang, M.; El-Rassi, G. D.; Metzinger, K.; Smith, B. J.; Lucas, E. A.; Clarke, S. L.; Chohanadisai, W.; Shen, X.; He, H.; Conway, T.; von Lintig, J.; Lin, D. Astaxanthin-Shifted Gut Microbiota Is Associated with Inflammation and Metabolic Homeostasis in Mice. *J. Nutr.* **2020**, *150*, 2687–2698.
- (49) Gao, Y.; Liu, F.; Li, R. W.; Li, C.; Xue, C.; Tang, Q. Microbial Composition and Co-occurrence Patterns in the Gut Microbial Community of Normal and Obese Mice in Response to Astaxanthin. *Front. Microbiol.* **2021**, *12*, 671271.
- (50) Song, R.; Xu, Y.; Jia, Z.; Liu, X.; Zhang, X. Integration of intestinal microbiota and metabolomics to elucidate different alleviation impacts of non-saponification and saponification astaxanthin pre-treatment on paracetamol-induced oxidative stress in rats. *Food Funct.* **2022**, *13*, 1860–1880.
- (51) Wang, J.; Su, L.; Zhang, L.; Zeng, J.; Chen, Q.; Deng, R.; Wang, Z.; Kuang, W.; Jin, X.; Gui, S.; Xu, Y.; Lu, X. Spirulina platensis aqueous extracts ameliorate colonic mucosal damage and modulate gut microbiota disorder in mice with ulcerative colitis by inhibiting inflammation and oxidative stress. *J. Zhejiang Univ. Sci. B* **2022**, *23*, 481–501.
- (52) Chandel, D.; Sharma, M.; Chawla, V.; Sachdeva, N.; Shukla, G. Isolation, characterization and identification of antigenotoxic and anticancerous indigenous probiotics and their prophylactic potential in experimental colon carcinogenesis. *Sci. Rep.* **2019**, *9*, 14769.
- (53) Herp, S.; Brugiroux, S.; Garzetti, D.; Ring, D.; Jochum, L. M.; Beutler, M.; Eberl, C.; Hussain, S.; Walter, S.; Gerlach, R. G.; Ruscheweyh, H. J.; Huson, D.; Sellin, M. E.; Slack, E.; Hanson, B.; Loy, A.; Baines, J. F.; Rausch, P.; Basic, M.; Bleich, A.; Berry, D.; Stecher, B. Mucispirillum schaedleri Antagonizes Salmonella Virulence to Protect Mice against Colitis. *Cell Host Microbe* **2019**, *25*, 681–694.
- (54) Cani, P. D.; Depommier, C.; Derrien, M.; Everard, A.; de Vos, W. M. Akkermansia muciniphila: paradigm for next-generation beneficial microorganisms. *Nat. Rev. Gastroenterol. Hepatol.* **2022**, *19*, 625–637.
- (55) Plovier, H.; Everard, A.; Druart, C.; Depommier, C.; Van Hul, M.; Geurts, L.; Chilloux, J.; Ottman, N.; Duparc, T.; Lichtenstein, L.; Myrtdakis, A.; Delzenne, N. M.; Kluevink, J.; Bhattacharjee, A.; van der Ark, K. C.; Aalvink, S.; Martinez, L. O.; Dumas, M. E.; Maiter, D.; Loumaye, A.; Hermans, M. P.; Thissen, J. P.; Belzer, C.; de Vos, W. M.; Cani, P. D. A purified membrane protein from Akkermansia muciniphila or the pasteurized bacterium improves metabolism in obese and diabetic mice. *Nat. Med.* **2017**, *23*, 107–113.
- (56) Luo, J.; Wang, Z.; Fan, B.; Wang, L.; Liu, M.; An, Z.; Zhao, X. A comparative study of the effects of different fucoidans on cefoperazone-induced gut microbiota disturbance and intestinal inflammation. *Food Funct.* **2021**, *12*, 9087–9097.
- (57) Leung, C.; Rivera, L.; Furness, J. B.; Angus, P. W. The role of the gut microbiota in NAFLD. *Nat. Rev. Gastroenterol. Hepatol.* **2016**, *13*, 412–425.
- (58) Zhou, L.; Fang, L.; Sun, Y.; Su, Y.; Zhu, W. Effects of the dietary protein level on the microbial composition and metabolomic profile in the hindgut of the pig. *Anaerobe* **2016**, *38*, 61–69.
- (59) Lebeer, S.; Vanderleyden, J.; De Keersmaecker, S. C. Genes and molecules of lactobacilli supporting probiotic action. *Microbiol. Mol. Biol. Rev.* **2008**, *72*, 728–764.
- (60) Li, Y.; Zhang, Y.; Wei, K.; He, J.; Ding, N.; Hua, J.; Zhou, T.; Niu, F.; Zhou, G.; Shi, T.; Zhang, L.; Liu, Y. Review: Effect of Gut Microbiota and Its Metabolite SCFAs on Radiation-Induced Intestinal Injury. *Front. Cell Infect. Microbiol.* **2021**, *11*, 577236.
- (61) Li, Y.; Dong, J.; Xiao, H.; Zhang, S.; Wang, B.; Cui, M.; Fan, S. Gut commensal derived-valeric acid protects against radiation injuries. *Gut Microbes* **2020**, *11*, 789–806.
- (62) Zhao, T. S.; Xie, L. W.; Cai, S.; Xu, J. Y.; Zhou, H.; Tang, L. F.; Yang, C.; Fang, S.; Li, M.; Tian, Y. Dysbiosis of Gut Microbiota Is Associated With the Progression of Radiation-Induced Intestinal Injury and Is Alleviated by Oral Compound Probiotics in Mouse Model. *Front. Cell Infect. Microbiol.* **2021**, *11*, 717636.

(63) Ding, X.; Li, Q.; Li, P.; Chen, X.; Xiang, L.; Bi, L.; Zhu, J.; Huang, X.; Cui, B.; Zhang, F. Fecal microbiota transplantation: A promising treatment for radiation enteritis? *Radiother. Oncol.* **2020**, *143*, 12–18.

(64) Yang, J.; Zhou, Q.; Huang, Z.; Gu, Z.; Cheng, L.; Qiu, L.; Hong, Y. Mechanisms of in vitro controlled release of astaxanthin from starch-based double emulsion carriers. *Food Hydrocoll* **2021**, *119*, 106837.

(65) Fu, K.; Harrell, R.; Zinski, K.; Um, C.; Jaklenec, A.; Frazier, J.; Lotan, N.; Burke, P.; Klibanov, A. M.; Langer, R. A potential approach for decreasing the burst effect of protein from PLGA microspheres. *J. Pharm. Sci.* **2003**, *92*, 1582–1591.

(66) Han, X.; Guo, J.; You, Y.; Yin, M.; Ren, C.; Zhan, J.; Huang, W. A fast and accurate way to determine short chain fatty acids in mouse feces based on GC-MS. *J. Chromatogr. B Analyt. Technol. Biomed. Life Sci.* **2018**, *1099*, 73–82.

(67) Zhang, S.; Wang, H.; Zhu, M. J. A sensitive GC/MS detection method for analyzing microbial metabolites short chain fatty acids in fecal and serum samples. *Talanta* **2019**, *196*, 249–254.

(68) Hsu, Y. L.; Chen, C. C.; Lin, Y. T.; Wu, W. K.; Chang, L. C.; Lai, C. H.; Wu, M. S.; Kuo, C. H. Evaluation and Optimization of Sample Handling Methods for Quantification of Short-Chain Fatty Acids in Human Fecal Samples by GC-MS. *J. Proteome Res.* **2019**, *18*, 1948–1957.